NASA CONTRACTOR REPORT





NASA CR-2740

# EFFECT OF INLET TEMPERATURE AND PRESSURE ON EMISSIONS FROM A PREMIXING GAS TURBINE PRIMARY ZONE COMBUSTOR

*Gerald Roffe*

*Prepared by*
GENERAL APPLIED SCIENCE LABORATORIES, INC.
Westbury, N. Y. 11590
*for Lewis Research Center*

NATIONAL AERONAUTICS AND SPACE ADMINISTRATION • WASHINGTON, D. C. • SEPTEMBER 1976

| 1. Report No. | 2. Government Accession No. | 3. Recipient's Catalog No. |
|---|---|---|
| NASA CR-2740 | | |

| 4. Title and Subtitle | 5. Report Date |
|---|---|
| EFFECT OF INLET TEMPERATURE AND PRESSURE ON EMISSIONS FROM A PREMIXING GAS TURBINE PRIMARY ZONE COMBUSTOR | September 1976 |
| | 6. Performing Organization Code |
| 7. Author(s) | 8. Performing Organization Report No. |
| Gerald Roffe | GASL TR 227 |
| | 10. Work Unit No. |
| 9. Performing Organization Name and Address | |
| General Applied Science Laboratories, Inc.<br>Merrick and Stewart Avenues<br>Westbury, New York 11590 | 11. Contract or Grant No.<br>NAS3-18563 |
| | 13. Type of Report and Period Covered |
| 12. Sponsoring Agency Name and Address | Contractor Report |
| National Aeronautics and Space Administration<br>Washington, D.C. 20546 | 14. Sponsoring Agency Code |

15. Supplementary Notes

Final Report. Project Manager, Cecil J. Marek, Airbreathing Engines Division, NASA Lewis Research Center, Cleveland, Ohio

16. Abstract

Experiments were conducted to determine the performance of a premixing prevaporizing gas turbine primary zone combustor design over a range of combustor inlet temperatures from 700 to 1000 K and a range of inlet pressures from 40 to 240 $N/cm^2$. The 1 meter long combustor could be operated at pressures up to and including 120 $N/cm^2$ without autoignition in the premixing duct or flashback from the stabilized combustion zone. Autoignition occurred in the mixer tube at the 240 $N/cm^2$ pressure level with an entrance temperature of 830 K and a mixer residence time of 4 msec. Measured $NO_x$ level, combustion inefficiency, and hydrocarbon emission index correlated well with adiabatic flame temperature. $NO_x$ levels varied from approximately 0.2 to 2.0 g $NO_2$/kg fuel at combustion inefficiencies from 4 to 0.04 percent, depending upon adiabatic flame temperature and pressure. Measured $NO_x$ levels were sensitive to pressure, but did not follow the $p^{1/2}$ law as commonly assumed. Tests were made at equivalence ratios ranging from 0.35 to 0.65. The overall total pressure drop for the configuration varied slightly with reference velocity and equivalence ratio, but never exceeded 3 percent.

| 17. Key Words (Suggested by Author(s)) | 18. Distribution Statement |
|---|---|
| Premixing<br>Prevaporization<br>Combustion<br>Oxides of nitrogen<br>Gas turbine combustors | Unclassified - unlimited<br>STAR category 07 |

| 19. Security Classif. (of this report) | 20. Security Classif. (of this page) | 21. No. of Pages | 22. Price* |
|---|---|---|---|
| Unclassified | Unclassified | 47 | $4.00 |

* For sale by the National Technical Information Service, Springfield Virginia 22161

TABLE OF CONTENTS

## LIST OF FIGURES

LIST OF FIGURES (Continued)



APPENDIX

# INTRODUCTION

Considerable effort has been expended in recent years on the problem of reducing undesirable emissions from gas turbine combustors. Although emission control must be considered over the entire spectrum of gas turbine operation, particular emphasis has been placed on the condition encountered in the combustor of an aircraft engine during supersonic cruise. Supersonic cruise, where the combustor inlet air temperature is 833K (1500°R) and the pressure is 40 $N/cm^2$ (4 atmospheres), constitutes one of the more critical phases of the overall emission control problem. The extremely high combustor temperatures corresponding to this condition exacerbate the problem of controlling the production of nitrogen oxides*. Moreover, the fact that supersonic cruise occurs at high altitude intensifies the importance of $NO_x$ control due to the potentially adverse affect of $NO_x$ emissions on the stratospheric ozone layer.

A number of techniques have been proposed for limiting the production of $NO_x$ in gas turbine combustors. Several of these (lean primary zone, rapid quench, two stage combustion) have shown considerable promise when incorporated into operating gas turbines and have reduced $NO_x$ emission levels to the order of 4 g-$NO_2$/kg-fuel (References 1-3) with combustion efficiencies of at least 99%. However, the technique which has demonstrated the most impressive ability to reduce $NO_x$ emission is that of premixed combustion which, in flame tube experiments (References 4-6), has achieved emission levels as low as 0.2 g-$NO_2$/kg-fuel at the supersonic cruise condition with 99% combustion efficiency. To date, premixed combustion has not been incorporated into an operating gas turbine engine.

In work performed recently at General Applied Science Laboratories, Inc., (References 6 and 7) a number of premixing combustor designs were tested at the supersonic cruise condition to determine the effect of premixing quality on combustor emission levels. One particular design, utilizing the normal injection of liquid fuel through a number of orifices mounted flush with the walls of a premixing tube, produced particularly low levels of $NO_x$, CO and un-

---

*NO and $NO_2$, the sum of which is generally designated as $NO_x$.

burned hydrocarbons (UHC). As a result, it is possible that this concept can serve as the kernel of a second generation low emission combustor design. However, before such a scheme can be considered for integration within an operating engine, additional information is required regarding its performance at conditions other than the single point at which tests were conducted. In this experiment, two specific performance characteristics were ascertained. First, the variation of $NO_x$, CO and UHC emission levels with combustor entrance temperature and pressure. Second, whether the concept could be used at the high pressures and temperatures encountered in takeoff and climb-out without encountering flashback or autoignition in the premixing tube.

This report presents the results of an experimental program in which the GASL normal injection premixing burner was operated over a range of temperatures between 700K and 1000K at pressures of 40, 80, 120 and 240 $N/cm^2$. The combustor reference velocity, defined as the mass flow rate divided by the combustor entrance density and maximum cross sectional area was held constant at 43 m/sec (150 ft/sec). The combustor section of the flame tube apparatus was 15.2 cm (6-inches) in diameter and 46 cm (18-inches) in length. The Mach number in the mixer tube, which varied slightly with entrance temperature to maintain a fixed reference velocity, was 0.25 at the supersonic cruise temperature (833K) which is representative of the compressor exit Mach number. The flame tube apparatus represents the primary zone of a combustor without secondary air dilution. Consequently, the exit temperatures are higher than those for a complete combustor.

## TEST APPARATUS AND PROCEDURES

### Combustor Test Rig

The combustor test apparatus is illustrated in Figure (1). Heated air enters the 8.9 cm diameter mixing duct through a bell mouth transition from an upstream plenum chamber. Fuel is injected through a set of flush mounted wall orifices located 15 cm from the entrance face. The fuel and air mix and flow through the premixing duct at a velocity of 135 m/sec and over a $10^o$ half angle, hollow-based, conical flameholder supported by four hollow-based struts at the combustor entrance station. The mixer duct diameter expands by 64% from

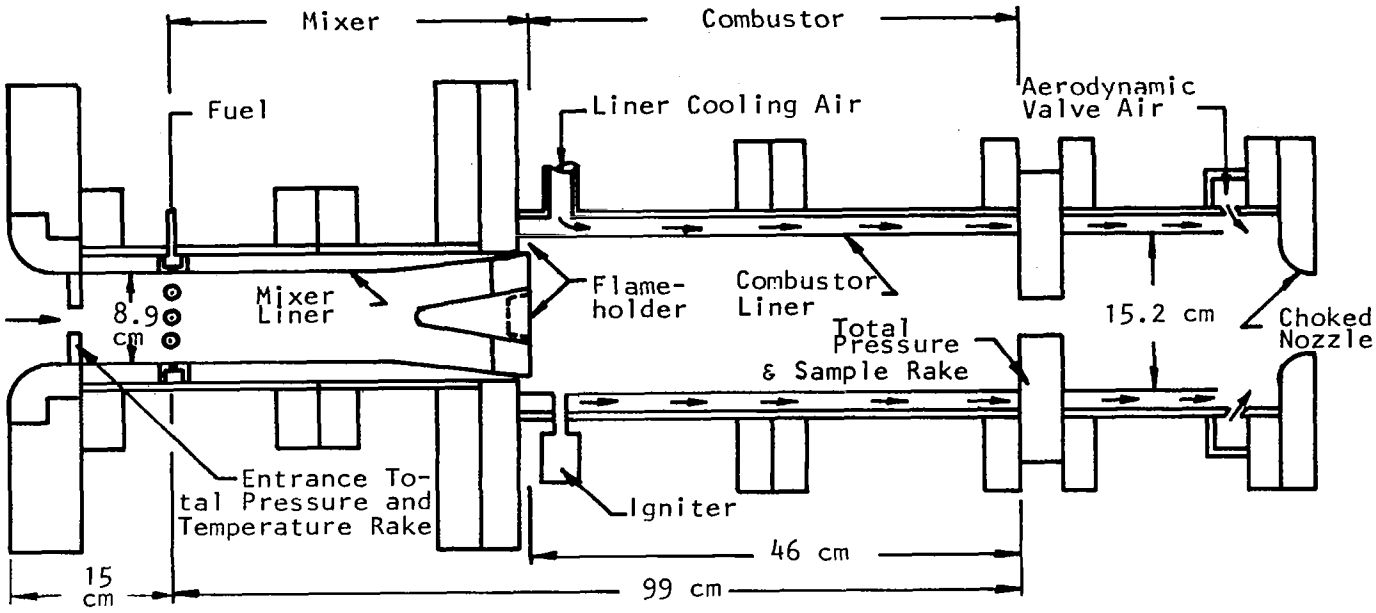


FIGURE 1. COMBUSTION TEST APPARATUS

the tip of the cone to the combustor entrance station to provide some diffusion of the high velocity air in order to reduce stagnation pressure losses associated with the sudden expansion and combustion which occurs downstream. The details of the flameholder section are shown in Figure (2).

The combustor flame is anchored by three connected recirculation regions: (i) the 5.1 cm diameter flameholder base, (ii) the 1.3 cm struts, and (iii) the separated flow at the 1.9 cm annular step at the combustor entrance. The combustor is cylindrical with a diameter of 15.2 cm and a length of 46 cm. The combustor exit station is equipped with a water cooled cruciform rake containing sixteen sampling ports located at the centers of equal flow areas. The legs of the sampling rake are offset by $45^{o}$ from the legs of the flameholder. A hydrogen-air gas igniter initiates combustion at a point just downstream of the annular step and is shut off once ignition is achieved.

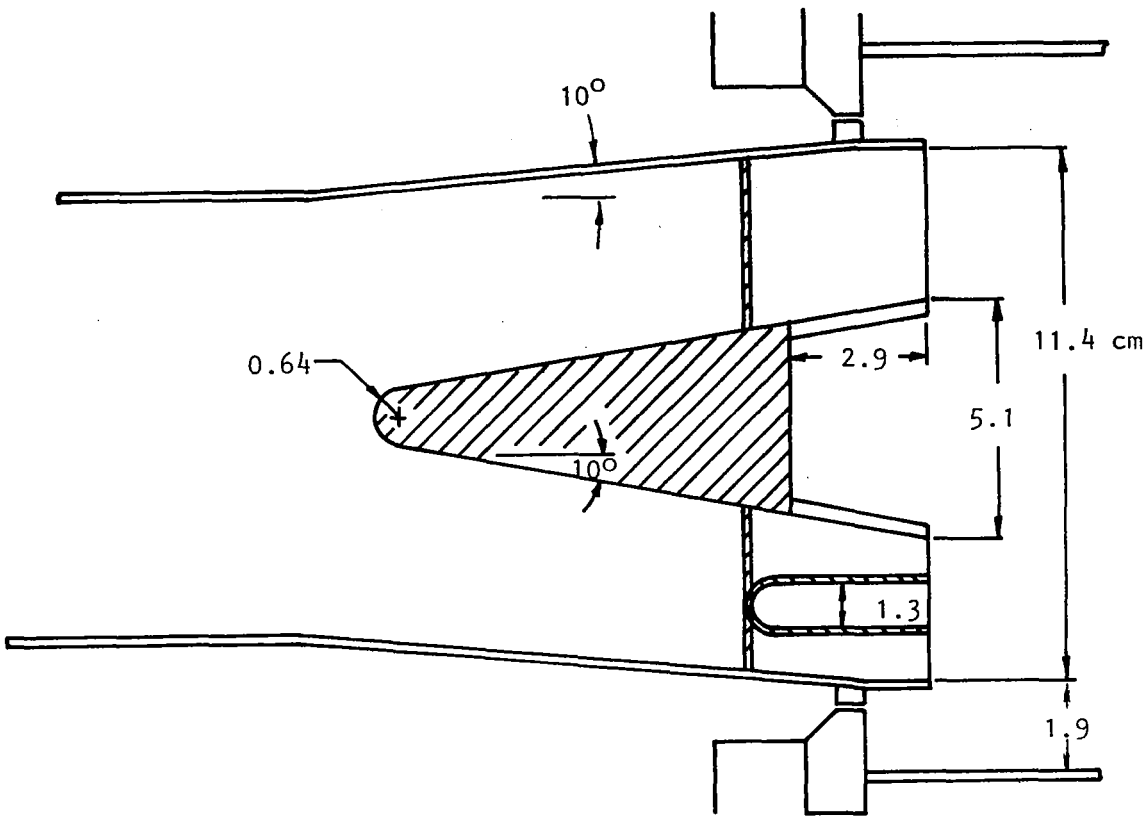


FIGURE 2. FLAMEHOLDER DETAILS

The details of the fuel injection assembly are illustrated in Figure (3) Twelve flush mounted orifices are set into a ring plenum and spray fine jets of fuel across the mixer airstream. Each transverse jet of fuel is atomized by the shear of the surrounding air to create a sheet of fine droplets which need only diffuse through the small lateral distance between adjacent sheets to mix completely. The fuel injection scheme is simple and offers the substantial advantages of a good initial dispersion of the liquid and an aerodynamically clean mixer tube. As with any simple pressure atomization system, it suffers from the disadvantage of coupling the fuel distribution pattern with the flow rate. This coupling comes from the fact that the penetration of a fixed diameter transverse liquid jet is very nearly a linear function of the jet mass flow. As a result, the degree of premixing which can be produced falls off somewhat as the equivalence ratio decreases.

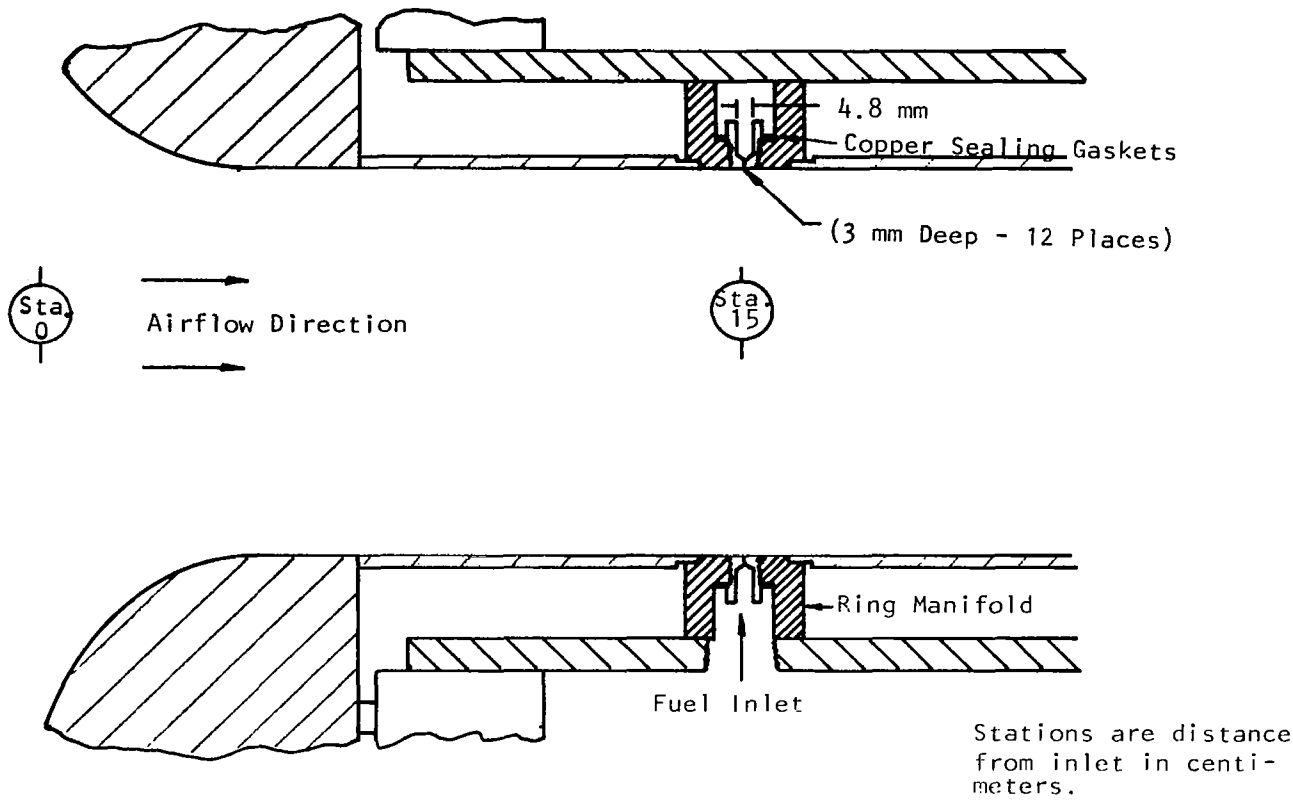


FIGURE 3. FUEL INJECTOR ASSEMBLY

Since tests were conducted at a constant reference velocity, the air mass flow varied by a factor of six between tests conducted at the lowest total pressure (40 $N/cm^2$) and those conducted at the highest (240 $N/cm^2$). The mass flow of fuel through a fixed diameter orifice varies with the square root of the orifice pressure drop. As a result, using the same fuel orifice diameter for tests at all pressures would be impractical. Therefore, the orifice diameter was held constant for all tests at the same total pressure but varied when the pressure level and total mass flow were changed. The fuel orifice diameters used are listed in Table I. Within the constraints of standard drill sizes the orifice area was varied in direct proportion to the mass flow.

The apparatus was constructed using a heavy outer shell for pressure containment and a lighter stainless steel liner to reduce the thermal stress on the pres-

TABLE I

FUEL ORIFICE DIAMETER

| Total Pressure ($N/cm^2$) | Total Temperature (K) | Orifice Diameter (mm) |
|---|---|---|
| 40 | All levels tested | 0.40 |
| 80 | All levels tested | 0.56 |
| 120 | All levels tested | 0.66 |
| 240 | All levels tested | 0.94 |

sure vessel. The gap between the pressure shell and the liner was sealed in the mixer section to insulate and minimize heat losses. In the combustor section, cold air was injected into the gap between the liner and the pressure wall as a means of limiting liner temperature and preventing mechanical failure. During operation, the mixer wall temperature was approximately 50 K lower than the burner inlet air temperature and the combustor liner temperature was approximately constant at a temperature of 1000 K, varying somewhat with equivalence ratio.

The exit of the combustion apparatus is a choked orifice, sized to produce a stagnation pressure of approximately 75% of the desired level at the design mass flow. The combustor liner cooling air is added to the combustor exhaust gas along with a separately controlled quantity of air which is injected just upstream of the exit orifice. The amount of additional air added upstream of the exit orifice is controlled to produce the desired combustor entrance stagnation pressure. This aerodynamic valve provides a means of maintaining constant combustor pressure as equivalence ratio and entrance temperature are varied.

## Fuel System and Properties

Liquid JP-5 fuel is stored in a tank which is pressurized with nitrogen and connected to the apparatus through a cavitating venturi and turbine flow meters. The flow rate is a function of the upstream pressure which is controlled by an in-line regulator. A physical analysis of the JP-5 used is presented in Table II.

TABLE II

JP-5 PHYSICAL ANALYSIS

| | |
|---|---|
| Specific gravity at 288K ($60^{o}$F) | 0.815 (42.1 deg. A.P.I.) |
| Flash point, PM | 329K ($134^{o}$F) |
| Pour point | 277K ($-50^{o}$F) |
| Viscosity at 310K ($100^{o}$F) | $1.5 \times 10^{-6}$ $m^2$/sec (31 sec. S.S.U.) |
| Initial boiling point | 452K ($355^{o}$F) |
| 10% Distillate | 469K ($385^{o}$F) |
| 20% Distillate | 477K ($400^{o}$F) |
| 50% Distillate | 499K ($440^{o}$F) |
| 90% Distillate | 544K ($520^{o}$F) |
| Final boiling point | 555K ($540^{o}$F) |
| Residue, by volume | 3% |

## Instrumentation

A 0.3 cm thick (12% blockage) rake spans the combustor entrance duct and defines mixer stagnation pressure and temperature. Static pressure taps and liner surface thermocouples are provided along the walls of the apparatus. Figure (4)

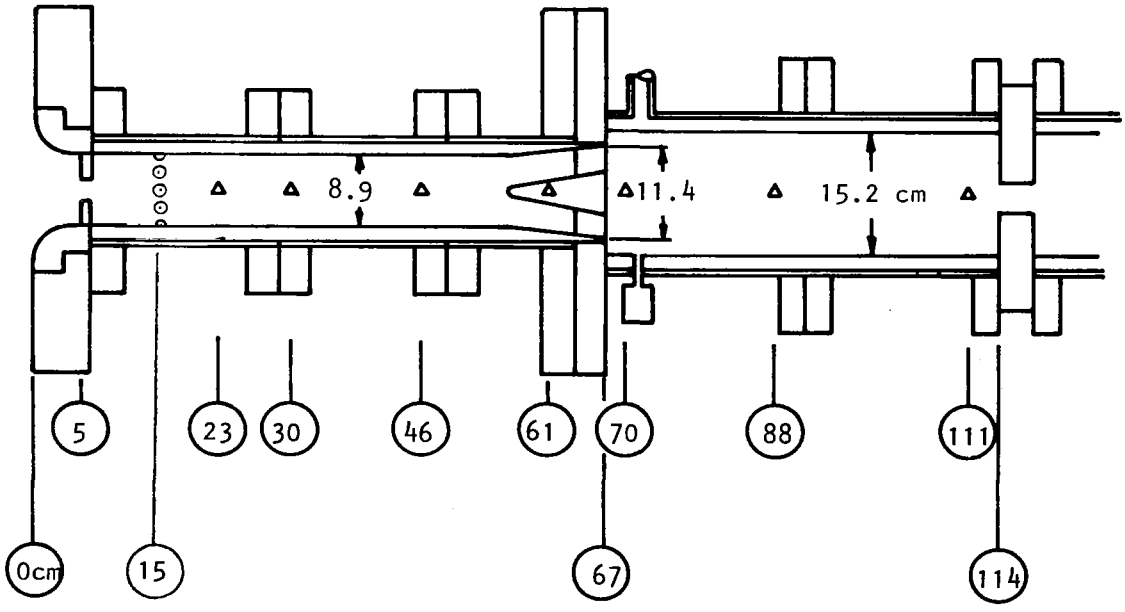


FIGURE 4. COMBUSTION APPARATUS - INSTRUMENTATION STATIONS DENOTED BY TRIANGLES - CIRCLED DIMENSIONS ARE AXIAL DISTANCE FROM ENTRANCE IN CENTIMETERS

summarizes the instrumentation locations and dimensions of the basic configurations.

A sixteen point cruciform sampling rake is located at the combustor exit station. The rake is constructed of stainless steel and is cooled by an internal flow of water which is discharged downstream to cool the combustor exhaust gas. The sixteen individual ports are located on four struts at the center of equal flow areas and are manifolded externally to provide an average gas sample for chemical analysis.

The gas sampling system is shown schematically in Figure (5). The sampling

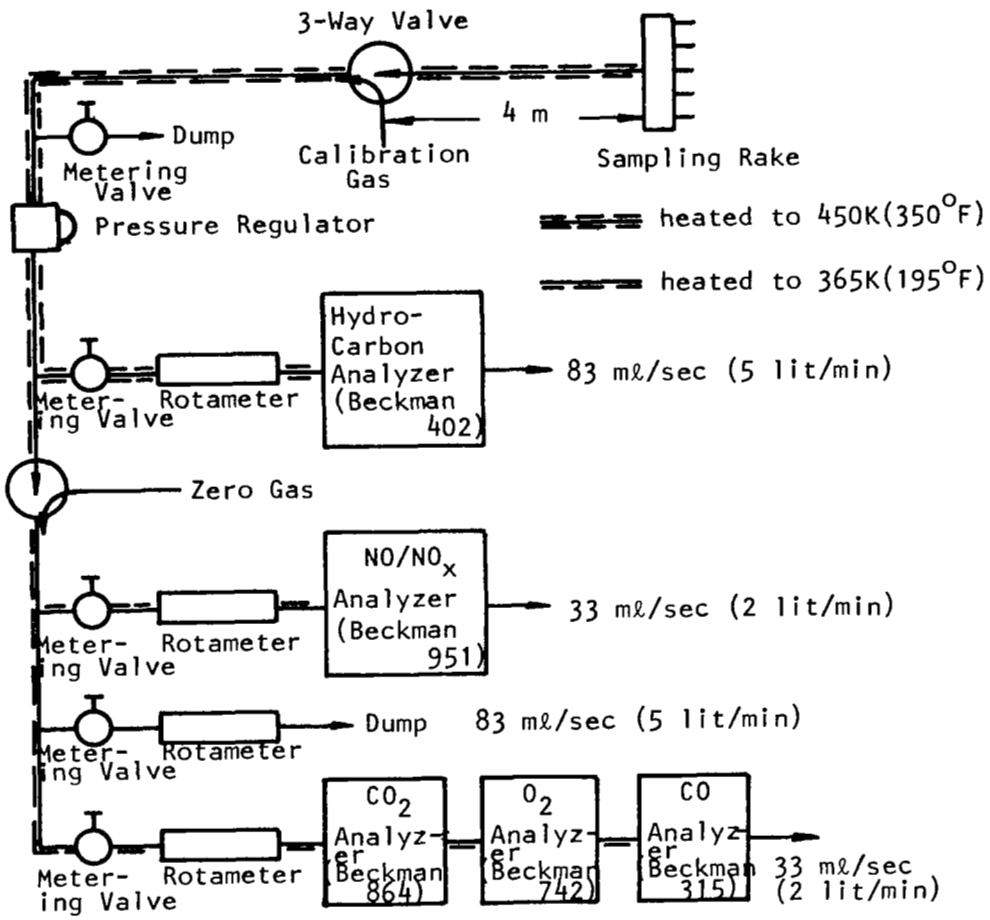


FIGURE 5. SAMPLING SYSTEM SCHEMATIC

manifold is connected by a 6.4 mm (1/4-inch) stainless steel line to a high flow pressure regulator and dump valve. The sample, collected at the combustor stagnation pressure is regulated down to a pressure of $2 \times 10^5$ N/m$^2$ (2 atm) before being divided by a set of metering valves into four individual streams. The sample line is heated to a temperature of 450K (350$^{\circ}$F) up to a Beckman Model 402 hydrocarbon analyzer which accepts one of these streams: the remaining three sample streams are allowed to cool to 365K (195$^{\circ}$F). The sample line is heated by wrapping it with an asbestos cloth resistance heater and enclosing the assembly with a fiberglass/plastic foam insulating sheath. One of the sample streams is passed through a Beckman Model 951 NO/NO$_x$ analyzer (chemiluminescence). Another leads to a Beckman Model 864 infrared analyzer ($CO_2$), a Beckman Model 742 oxygen analyzer (Polarographic) and a Beckman Model 315B infrared analyzer (CO), connected in series. The last line is used as a dump. Flow rates through the system are kept high by maximizing the amount of sample dumped both up and downstream of the pressure reduction regulator. Calibration gas is introduced through a three way valve located just downstream of the sample manifold. Zero gas for the oxygen, $CO_2$ and CO analyzers (dry nitrogen) enters through a three way valve located upstream of the set of metering valves. The NO/NO$_x$ and hydrocarbon analyzers provide internal sources of zero gas. Gas analysis procedures and data reduction equations were in accordance with ARP 1256, Reference (2). The data reduction procedures and instrument calibration curves are presented in Appendix A.

## Test Procedure

The experiments were carried out using the pebble bed blow-down facility of General Applied Science Laboratories, Inc., whose pertinent components are illustrated in Figure (6). Mechanical compressors fill a bank of storage bottles with air at a pressure on the order of $10^3$ N/cm$^2$. The air is dried prior to storage and contains less than $2 \times 10^{-4}$ kg of water per kg of air. Prior to a test, a bed of aluminum oxide pebbles is heated by electric glow-bars to a preset temperature. Air from the storage bank is passed through the bed of heated pebbles and into the combustion apparatus.

As with any blow-down facility, test time was limited by the heat storage capacity of the pebble bed and the air storage capacity of the tanks. For these

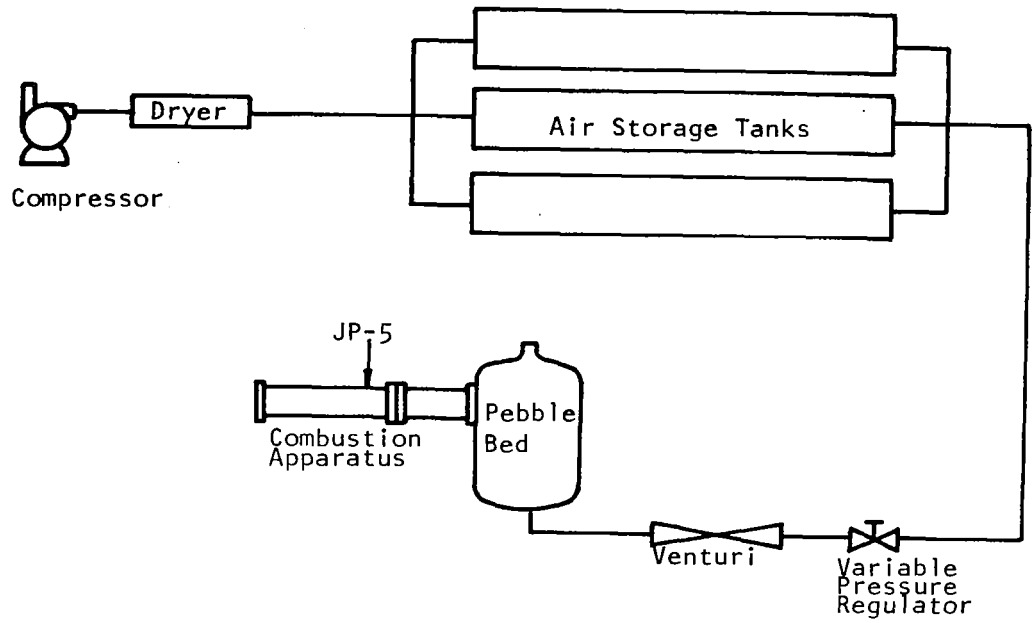


FIGURE 6. SCHEMATIC OF GASL PEBBLE BED COMBUSTION TEST FACILITY

tests, heat storage capacity was the limiting quantity. For tests at a pressure of 40 N/cm$^2$, the pebble bed outlet temperature holds within $\pm$ 6K (10$^\circ$R) limits for over three minutes. Since the gas analysis system response time is approximately thirty seconds, conditions for each test point were held steady for one minute. As a result, the pebble bed temperature was generally fixed at the desired value and a sequence of data points taken at various equivalence ratios. The pebble bed would then be allowed to cool for several minutes and a new sequence of data points taken at the lower inlet air temperature. A similar procedure was followed at pressures of 80 N/cm$^2$, with less points taken in each run.

For tests conducted at a pressure of 120 N/cm$^2$ the pebble bed outlet temperature would drop at a rate of approximately 12K per minute. For these tests, equivalence ratio was held constant during the data interval and the temperature was allowed to drop. The temperature variation over the thirty second sample analysis time was $\pm$ 3K about the mean value assigned to the data point.

At a pressure of 240 N/cm$^2$ the system mass flow was such as to cause a temperature drop of approximately 10K in thirty seconds. Tests at this pressure level produced only one data point per run.

## DISCUSSION OF RESULTS

### Autoignition

One of the principal concerns regarding the application of premixed combustion to gas turbine engines is the possibility of premature combustion in the mixing duct. This possibility arises from the fact that the temperature at the combustor entrance is above the autoignition point for most fuels. In principle, autoignition can be avoided by limiting the residence time in the mixing duct to a value less than the mixture ignition delay time. The degree of uncertainty associated with available ignition delay data and the fact that local equivalence ratio, which strongly influences ignition delay, varies along the length of the mixing duct makes an accurate prediction of ignition delay extremely difficult. Therefore, an important by-product of any premixed combustion experiment is a determination of whether the device can be operated at steady state over an extended pressure range without autoignition or flashback.

The premixing combustor tested here was operated extensively at a pressure of 40 $N/cm^2$ without experiencing autoignition, either in the mixing duct (residence time 4 msec) or in the combustor section. Combustion had to be initiated by the use of a small hydrogen/air gas igniter placed in the separated flow downstream of the combustor entrance step. Once lit, the combustor flame continued burning without the continued use of the igniter.

When the combustor pressure level was increased to 80 $N/cm^2$, the mixture autoignited in the combustor section at inlet temperatures in excess of 850K. In general, no temperature rise was detected in the mixing duct. However, after a routine inspection and reassembly of the apparatus, autoignition occurred in the mixing duct just downstream of a slip joint connecting the cylindrical section of the mixer with the expanding section surrounding the flameholder cone.

A nearly identical situation was encountered at a pressure of 120 $N/cm^2$; satisfactory operation in the mixing duct and autoignition in the combustor making the use of the gas igniter unnecessary. As at the lower pressure, one incident of autoignition occurred at the slip joint following a routine inspection and reassembly. A close inspection of the apparatus following this incident revealed that misalignment of the slip joint upon reassembly produced a step on

one side of the mixer. Since such a step creates a region of local separation and recirculation, its ability to provide sufficient residence time for autoignition is understandable. After a careful reassembly, further incidents of autoignition were not experienced at the 120 $N/cm^2$ pressure level.

All attempts to operate at a pressure of 240 $N/cm^2$ produced autoignition in the cylindrical section of the mixer tube. A substantial temperature rise was indicated as early as station (46), thirty one centimeters downstream of the fuel injection station. As the mixer geometry is aerodynamically clean in this region, the inability to operate at 240 $N/cm^2$ is a purely chemical kinetic effect. It is likely that the problem could be corrected by increasing the mixer tube velocity, but this was not attempted in the present program.

In some premixing designs, it is possible to avoid autoignition but encounter a similar problem as the result of flashback, defined as the upstream propagation of a flame from a stabilized source into a combustible mixture. In no instance was flashback observed in the apparatus tested here. Summarizing, an aerodynamically clean mixer duct with a residence time of 4 msec proved capable of operation at temperatures up to 920K and pressures up to 120 $N/cm^2$ without encountering autoignition. The presence of small regions of separated flow in the mixer leads to problems of autoignition. At a pressure of 240 $N/cm^2$, an entrance temperature as low as 832K produced autoignition. In no case did the flame flash upstream from the stabilized combustion zone into the mixer flow.

All raw and reduced data taken during the test program is tabulated, along with the corresponding test conditions, in Appendix B. For each combustor total pressure level, the data represents a three-dimensional array with respect to the two independent variables, entrance temperature and equivalence ratio.

### Variation of Emissions with Equilibrium Flame Temperature

For the moment, it would be more convenient if the data could be examined in terms of only one independent variable. Since the production of $NO_x$, the oxidation of trace hydrocarbon species, and the equilibration of CO are, to a great extent, post flame reactions, the adiabatic flame temperature, which is a function of both equivalence ratio and entrance temperature, assuming 100 percent

efficiency, seems a particularly attractive potential correlation parameter.

Figure (7) presents the measured emission index for oxides of nitrogen as a function of adiabatic flame temperature. Although the data at 40 $N/cm^2$ displays a good deal of scatter, the adiabatic flame temperature does appear to correlate the data reasonably well. $NO_x$ emission index is seen to be an exponentially increasing function of flame temperature which, for the range of temperatures between 1800K and 2200K covered here, varies by an order of magnitude from 0.2 to 2.0 g-$NO_2$/kg-fuel. The sensitivity of $NO_x$ level to flame temperature appears to be approximately the same at 40 $N/cm^2$ and 80 $N/cm^2$ but decreases somewhat at 120 $N/cm^2$. The $NO_x$ emission index decreased when the pressure was varied.

The reason for the substantial data scatter in evidence at 40 $N/cm^2$ is not completely clear, although an error analysis of the gas sampling procedure indicates that the scatter is not the result of instrument error. The scatter is also present in combustion inefficiency indicating possible changes in the fuel distribution. The extremely small fuel orifice size employed in the low pressure test series allowed periodic blockage of random orifices which could possibly have produced differing fuel injection patterns. It is also possible that the soft copper seals around the injection orifices allowed a degree of leakage which was significant compared with the very small injection area used at the lowest pressure and the leakage pattern changed as the apparatus was cycled in temperature.

The measured values of combustion inefficiency and hydrocarbon emission index are shown in Figures (8) and (9) as functions of the adiabatic flame temperature. Each appears to be reasonably well represented as an exponentially decreasing function of flame temperature. The combustion inefficiency varies between 0.5% and 1.0% for pressures of 80 and 120 $N/cm^2$. At 40 $N/cm^2$, the combustion inefficiency varies between 1% and 4%, considerably in excess of the values reported in Reference (1) for the same conditions. The reason for this increase in inefficiency are not immediately evident, but may be related to the slightly erratic nature of the combustion indicated by the degree of scatter. At 120 $N/cm^2$, the combustion inefficiency begins to increase sharply as the temperature drops below 1900K, behavior typical of incipient blowout. This behavior is not evident

FIGURE 7. VARIATION OF $NO_x$ EMISSION INDEX WITH ADIABATIC FLAME TEMPERATURE

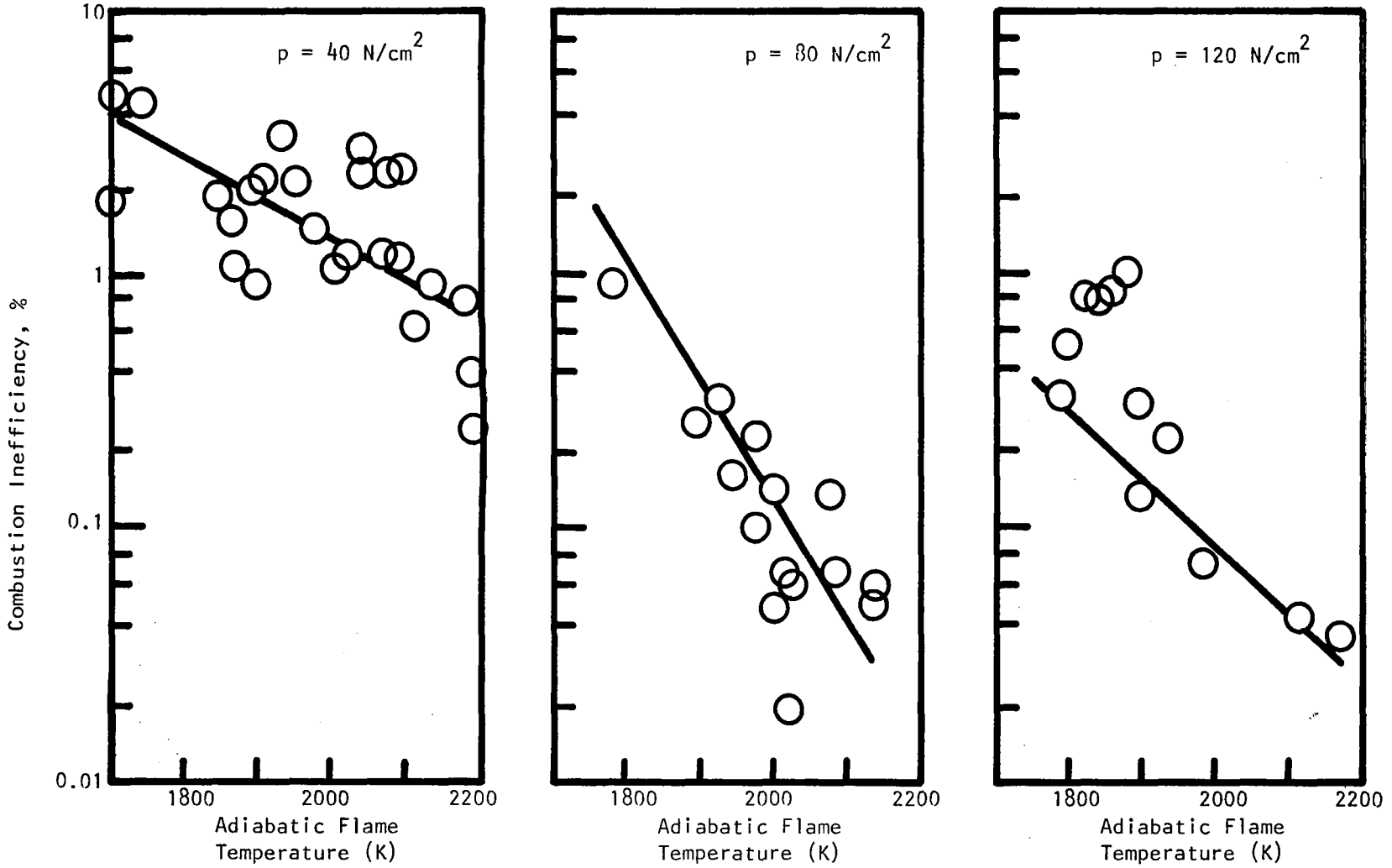


FIGURE 8. VARIATION OF COMBUSTION INEFFICIENCY WITH ADIABATIC FLAME TEMPERATURE

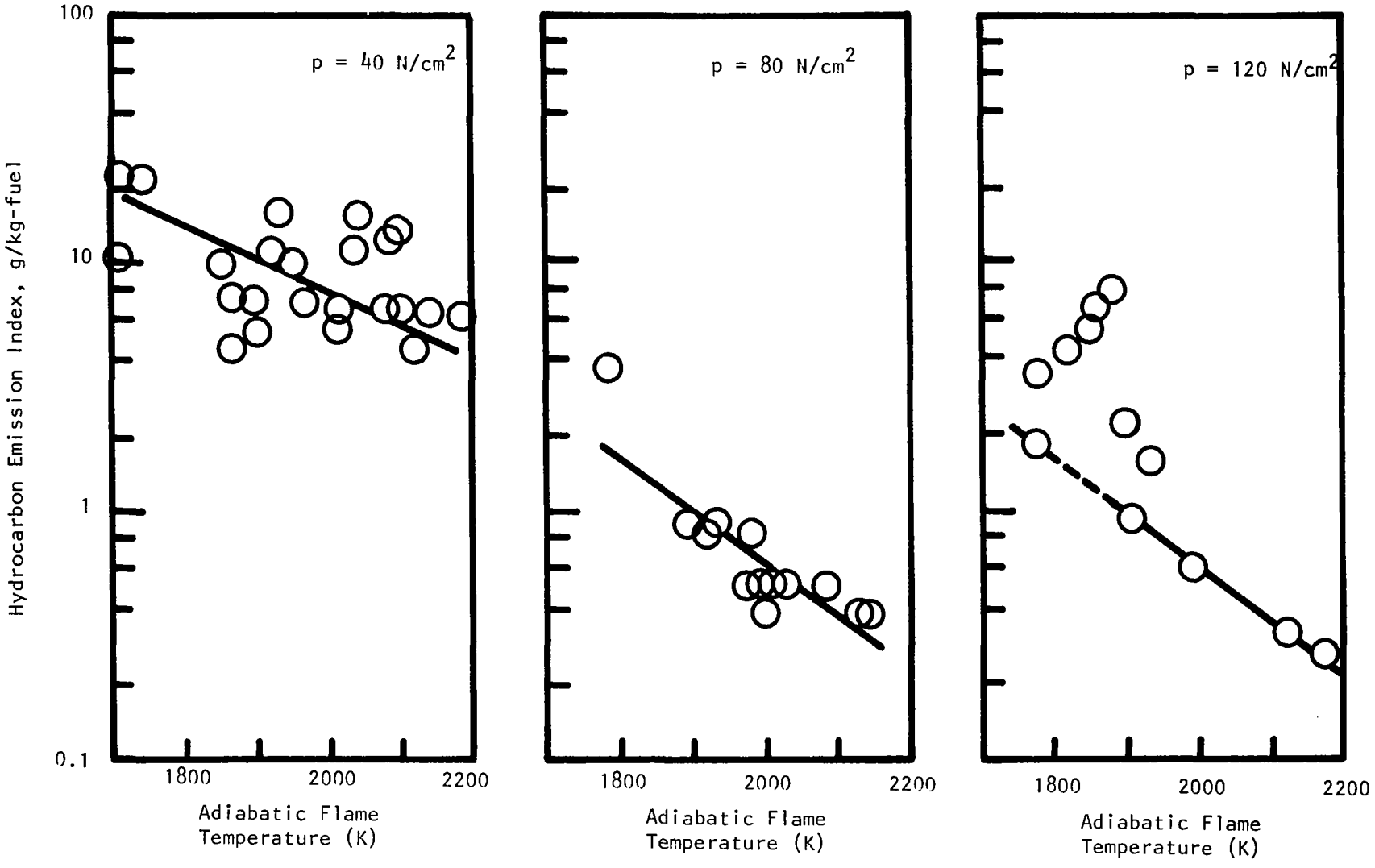


FIGURE 9. VARIATION OF HYDROCARBON EMISSION INDEX WITH ADIABATIC FLAME TEMPERATURE

at the lower pressures.

Figure (10) presents the difference between the measured concentration of carbon monoxide and the CO concentration corresponding to equilibrium at the pressure, equivalence ratio and adiabatic flame temperature for the test point. From the data of Figure (10), one would conclude that the CO level is approaching equilibrium with increasing rapidity as the pressure level increases. However, CO levels at 80 $N/cm^2$ are below equilibrium for adiabatic flame temperatures above 2000K (giving negative values of super-equilibrium concentration) and the same condition exists at 120 $N/cm^2$ at flame temperatures above 1900K. It is likely that this is the result of inadequate sample quench rates at the higher pressure levels where CO oxidation rates are higher.

By making use of the correlation with adiabatic flame temperature, the data can be presented as a function of the two independent variables, equivalence ratio and combustor entrance temperature. To do this, we make use of the fact that emission data taken at constant equivalence ratio (Reference 1) shows an entrance temperature dependence of the form

$$\ell n\, E_i = A_i + B_i T_3 \tag{1}$$

In this functional relationship $E_i$ represents either $NO_x$ or UHC emission index or combustion inefficiency, $T_3$ is the combustor entrance temperature and $A_i$ and $B_i$ are constants (or functions of equivalence ratio, $\phi$). This relationship can be used to correct data taken at one temperature, $T_3$, to an equivalent value at another temperature, $T_3'$, by the simple relation

$$E_i(T_3') = E_i(T_3)\, e^{B(T_3'-T_3)} \tag{2}$$

where B is simply the logarithmic derivative $\frac{\partial\, \ell n\, E_i}{\partial T_3}$.

Using Equation (2) all data can be corrected to the nearest 100K entrance temperature and plotted as a function of equivalence ratio. However, to do this we require the value of the derivative B. Fortunately, within the range of entrance temperature and equivalence ratio covered here, the adiabatic flame tem-

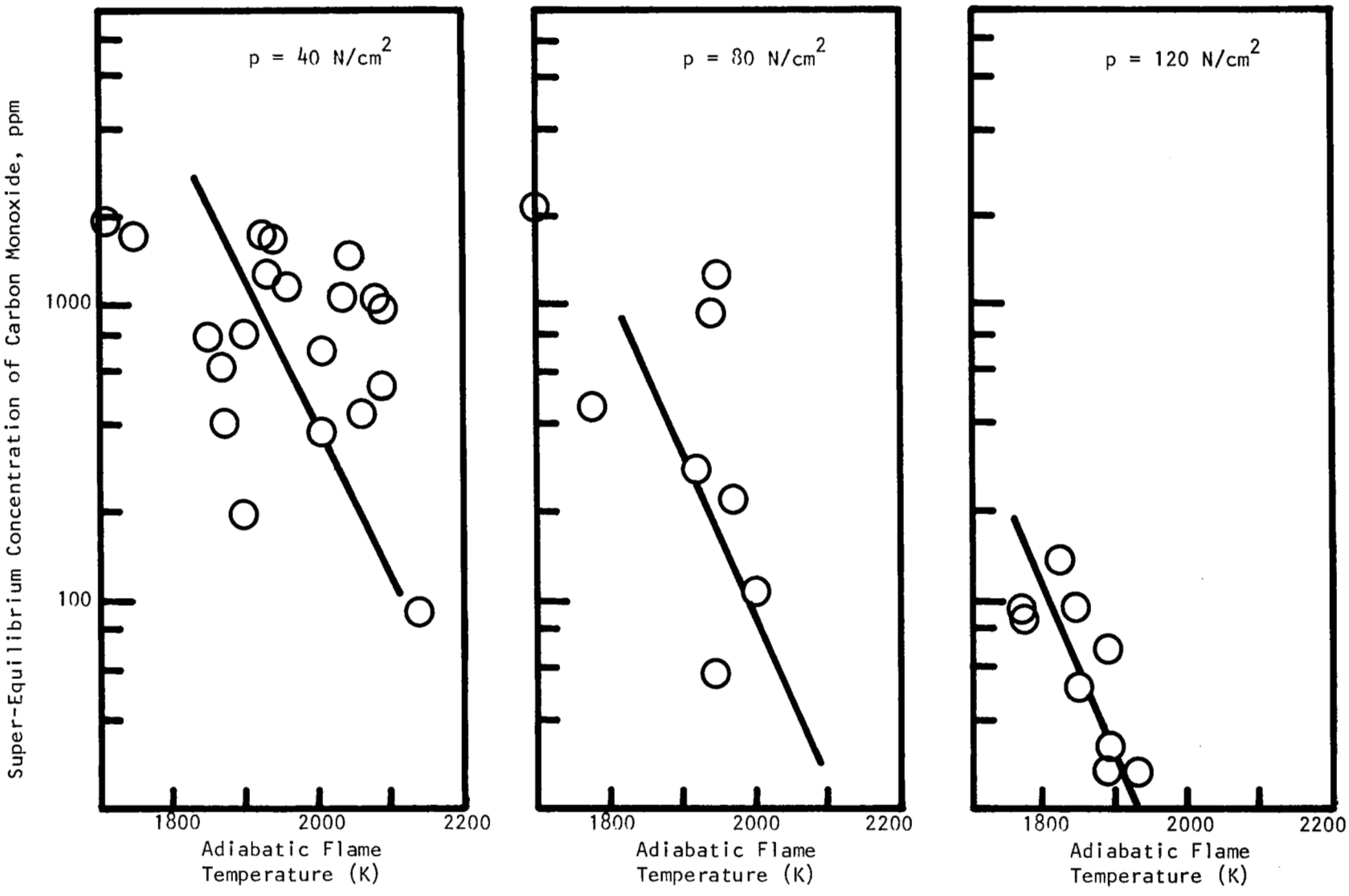


FIGURE 10. SUPER-EQUILIBRIUM CONCENTRATION OF CO AS A FUNCTION OF ADIABATIC FLAME TEMPERATURE

perature is well represented by the linear relation

$$T_4 = 1500 + 2000(\phi-0.25) + 0.9(T_3-900) \quad (3)$$

Combining Equations (3) and (1), differentiating at constant equivalence ratio and rearranging yields the result

$$B = 0.9 \frac{\partial \ell n\ E}{\partial T_4} \quad (4)$$

The derivative required in Equation (4) is simply the slope of the correlation curve already obtained.

## Variation of Emissions with Inlet Temperature, Equivalence Ratio, and Pressure

Equation (2) has been used to apply a limited correction to the reduced emission data to shift all points to the nearest multiple of one hundred degrees in entrance temperature. The maximum temperature correction is 50K. The magnitude of the correction factor applied to the data is a function of the slope of the adiabatic temperature correlation curve and the required temperature shift. However, for the most sensitive case ($NO_x$ emission index at a pressure of 40 $N/cm^2$) the maximum correction applied amounts to less than seven percent of full scale. As a result, the procedure is not highly sensitive to errors in the adiabatic temperature correlation.

Figures (11) through (13) present the combustor emission data, corrected to the nearest multiple of 100K inlet temperature as functions of inlet temperature and equivalence ratio. For a pressure of 40 $N/cm^2$, Figure (11) indicates that $NO_x$ level increases by an order of magnitude for a temperature increase of 200K. Combustion inefficiency and hydrocarbon emission index are both more sensitive to inlet temperature level, each requiring 263K for a decade increase. Increasing equivalence ratio produces the same result as increasing inlet temperature, driving $NO_x$ levels higher while dropping the hydrocarbon emission index and combustion inefficiency.

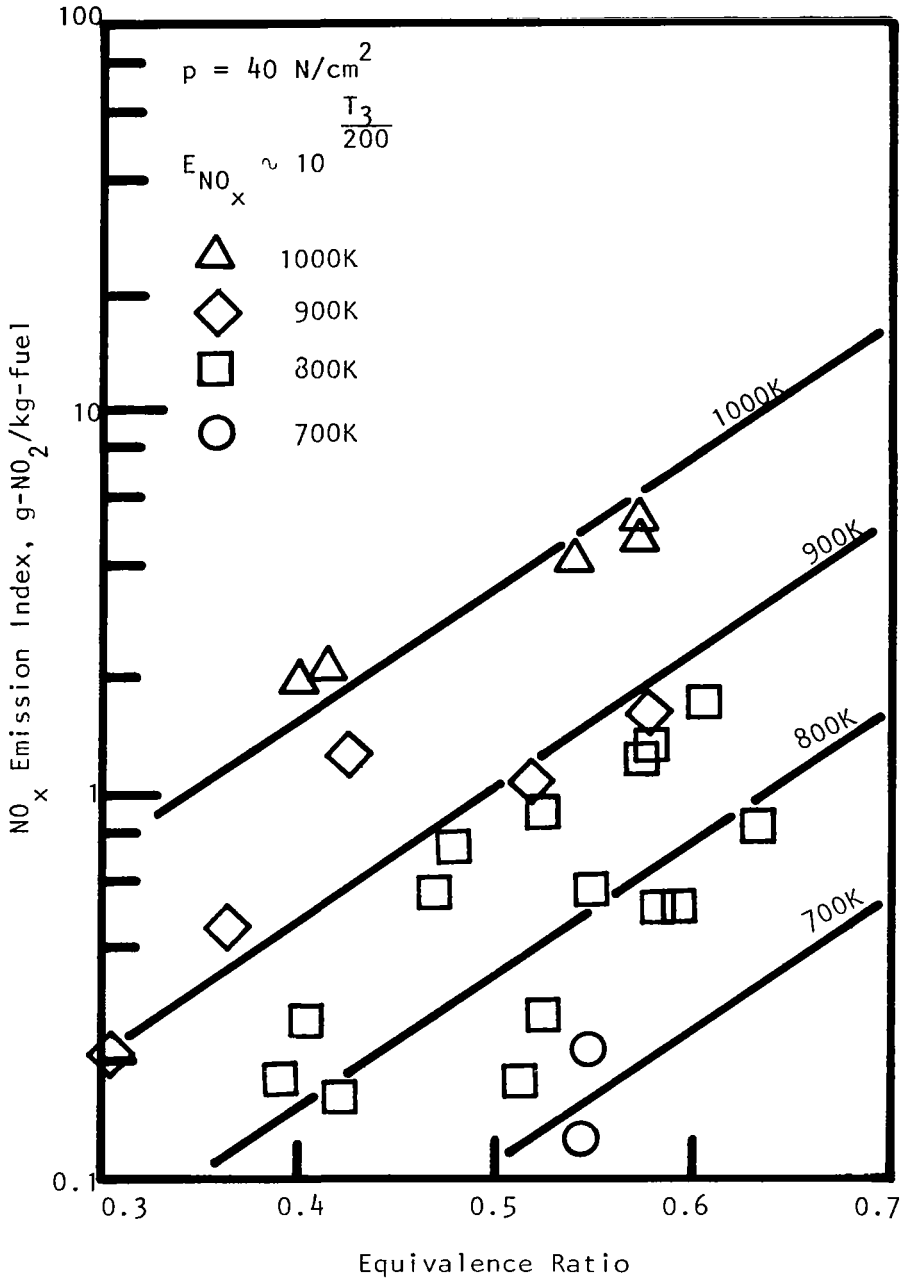


FIGURE 11a. $NO_x$ EMISSION INDEX AS A FUNCTION OF EQUIVALENCE RATIO AND COMBUSTOR INLET TEMPERATURE AT 40 N/cm$^2$

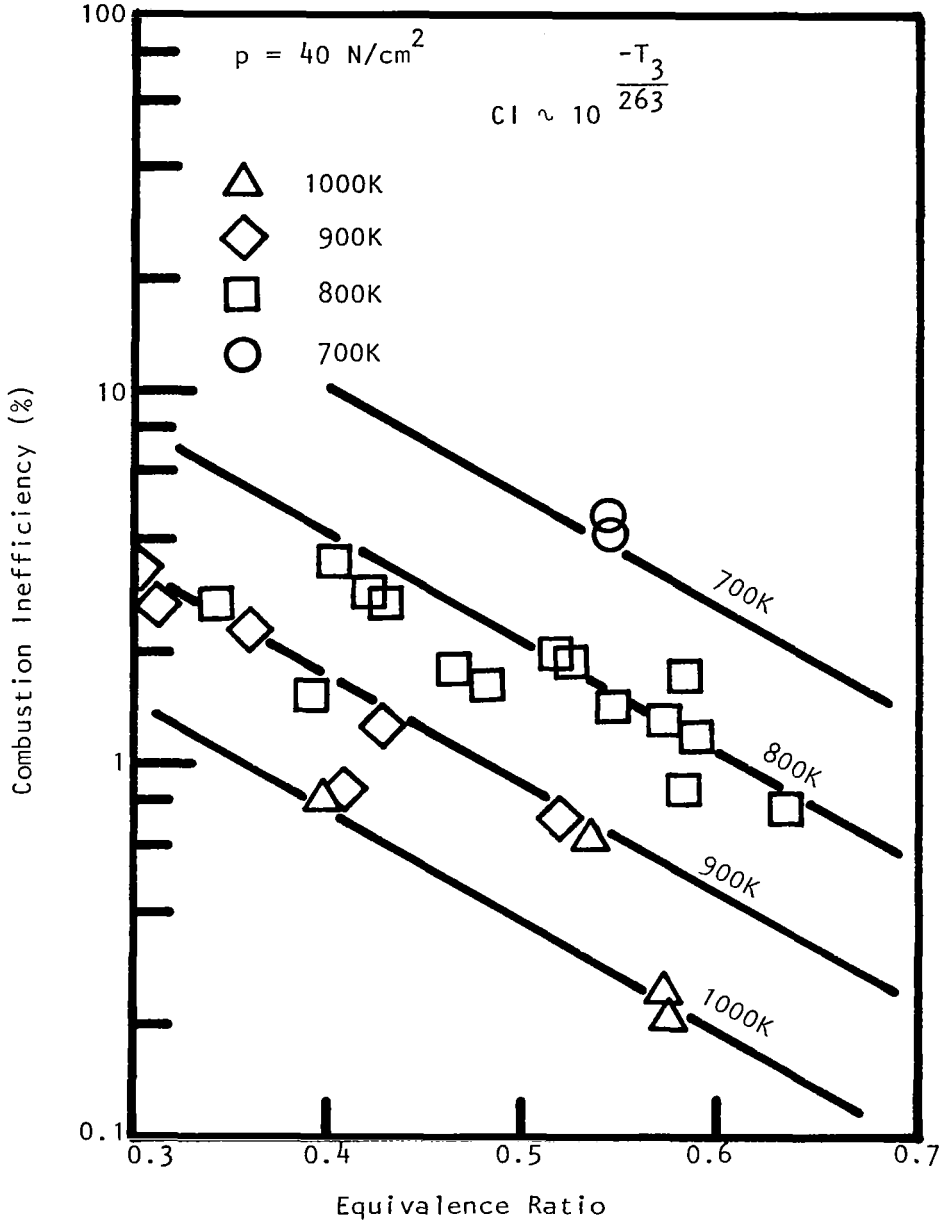


FIGURE 11b. COMBUSTION INEFFICIENCY AS A FUNCTION OF EQUIVALENCE RATIO AND COMBUSTION INLET TEMPERATURE AT 40 N/cm$^2$

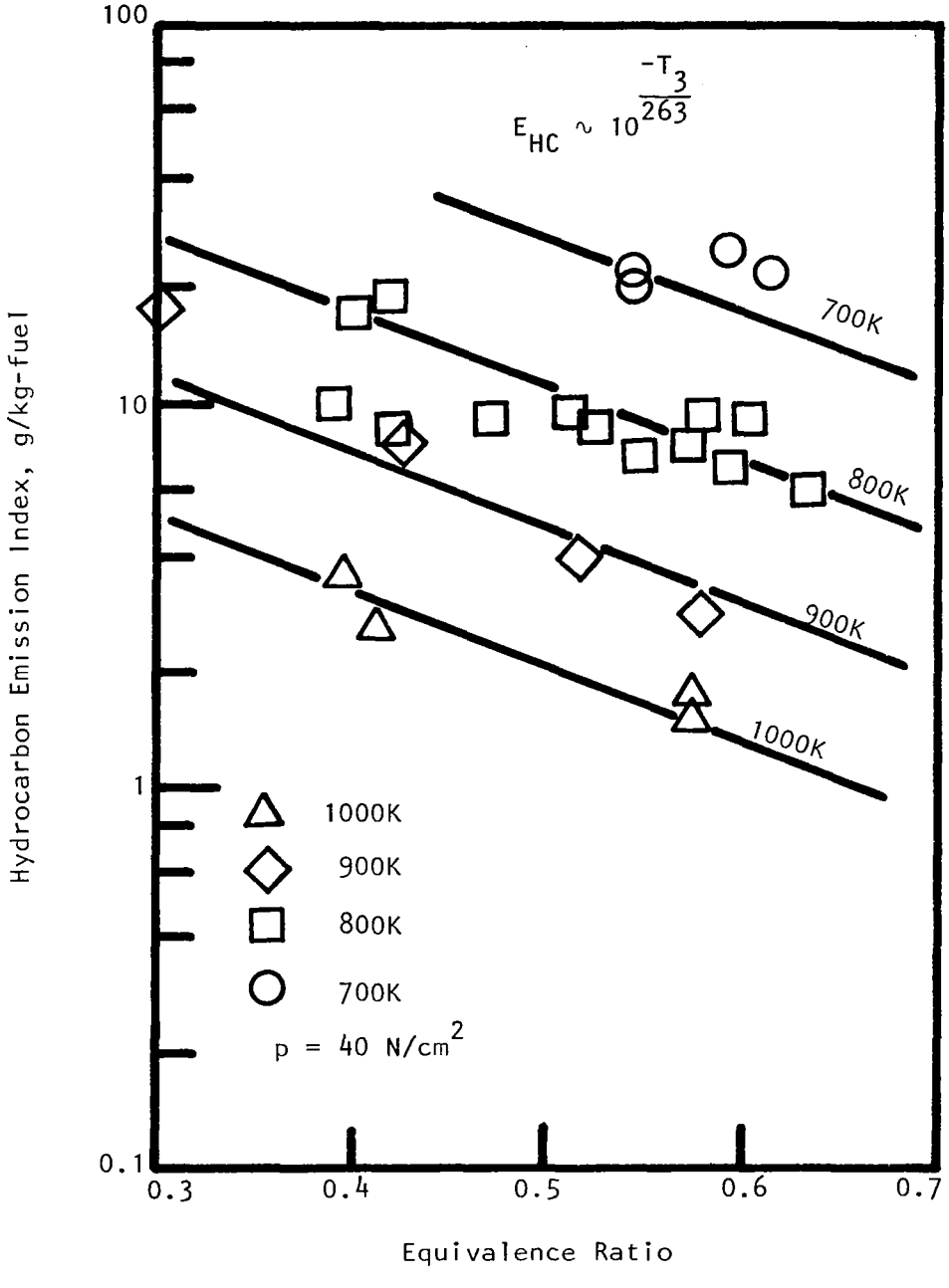


FIGURE 11c. HYDROCARBON EMISSION INDEX AS A FUNCTION OF EQUIVALENCE RATIO AND COMBUSTOR INLET TEMPERATURE AT 40 N/cm$^2$

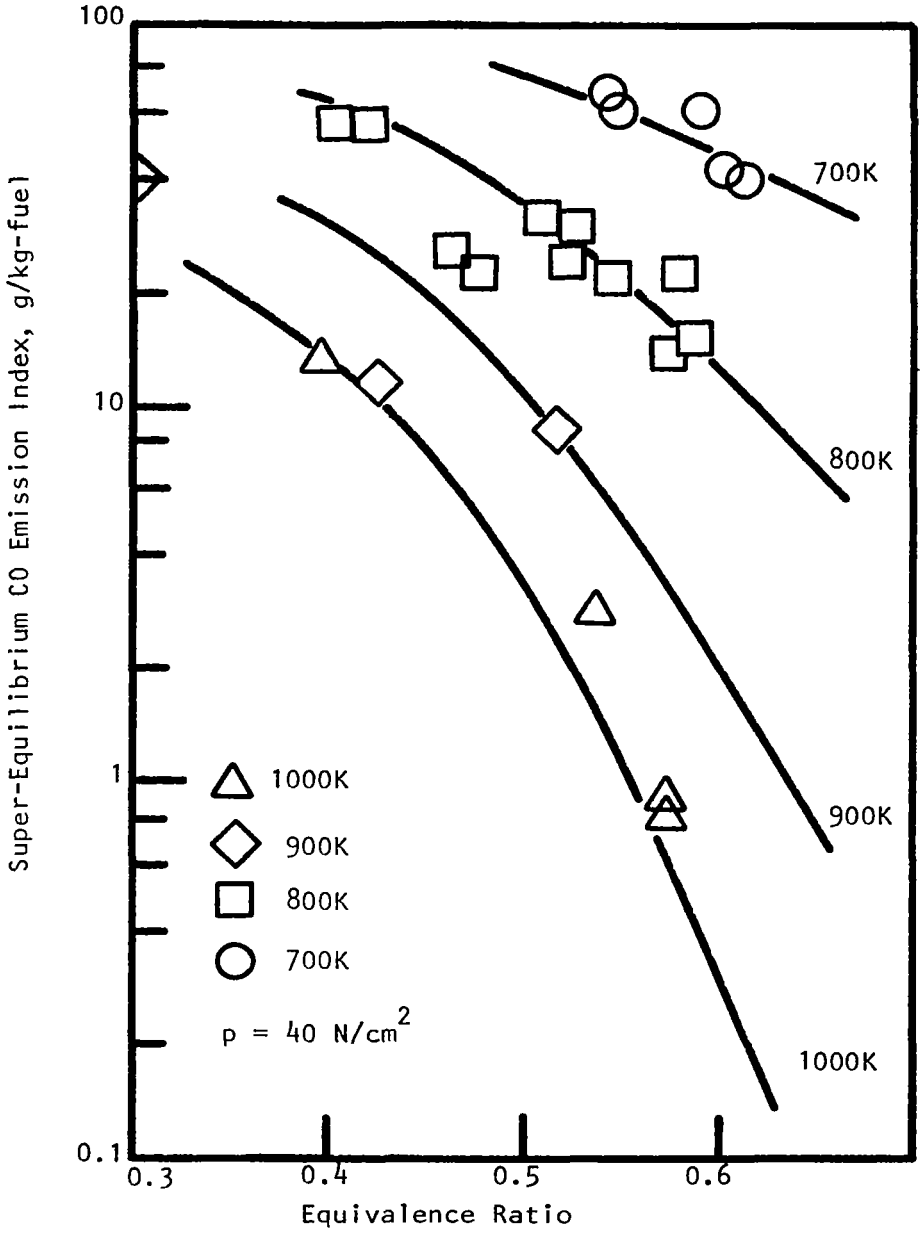


FIGURE 11d. SUPER-EQUILIBRIUM CARBON MONOXIDE EMISSION INDEX AS A FUNCTION OF EQUIVALENCE RATIO AND COMBUSTOR INLET TEMPERATURE AT 40 $N/cm^2$

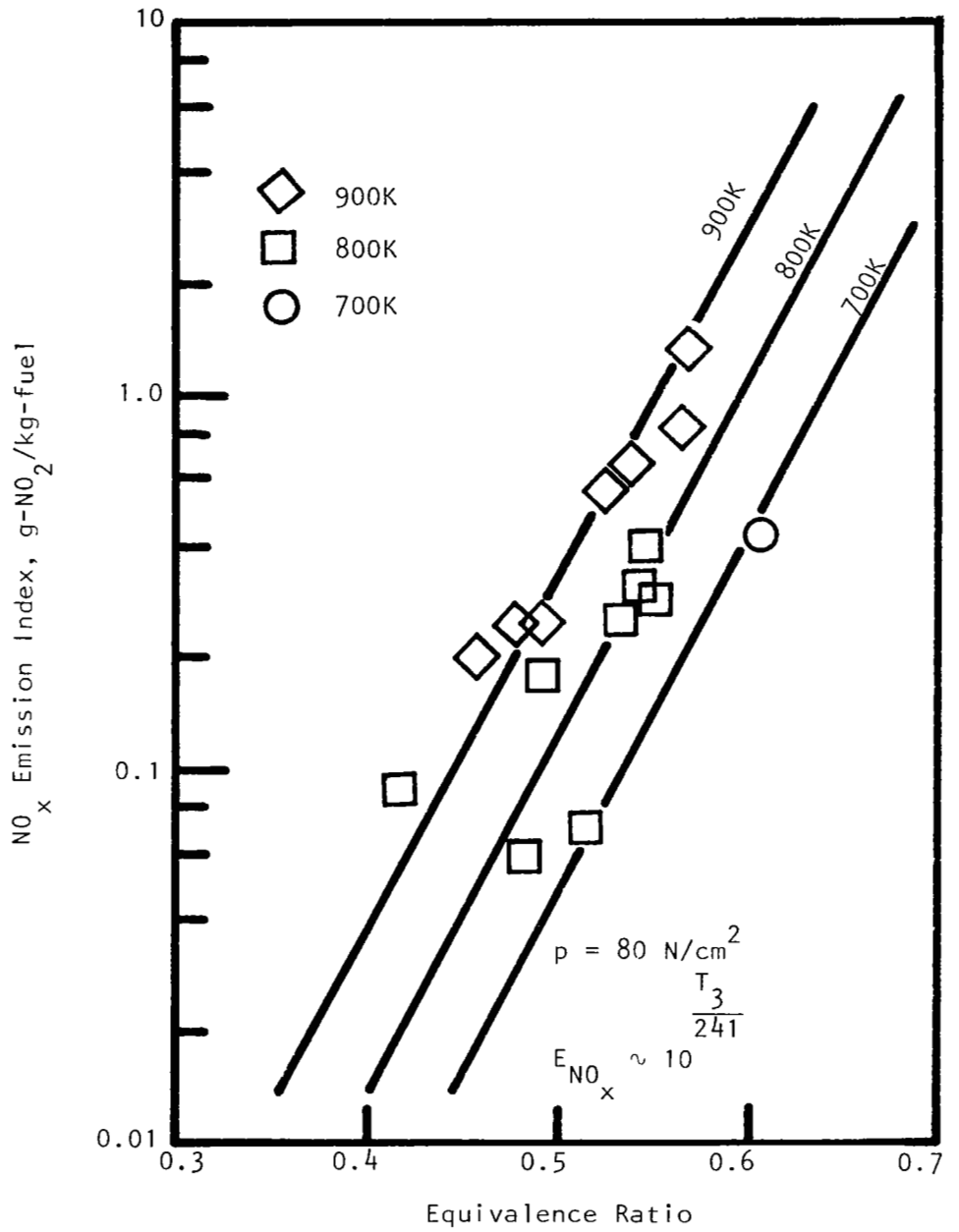


FIGURE 12a. $NO_x$ EMISSION INDEX AS A FUNCTION OF EQUIVALENCE RATIO AND COMBUSTOR INLET TEMPERATURE AT 80 $N/cm^2$

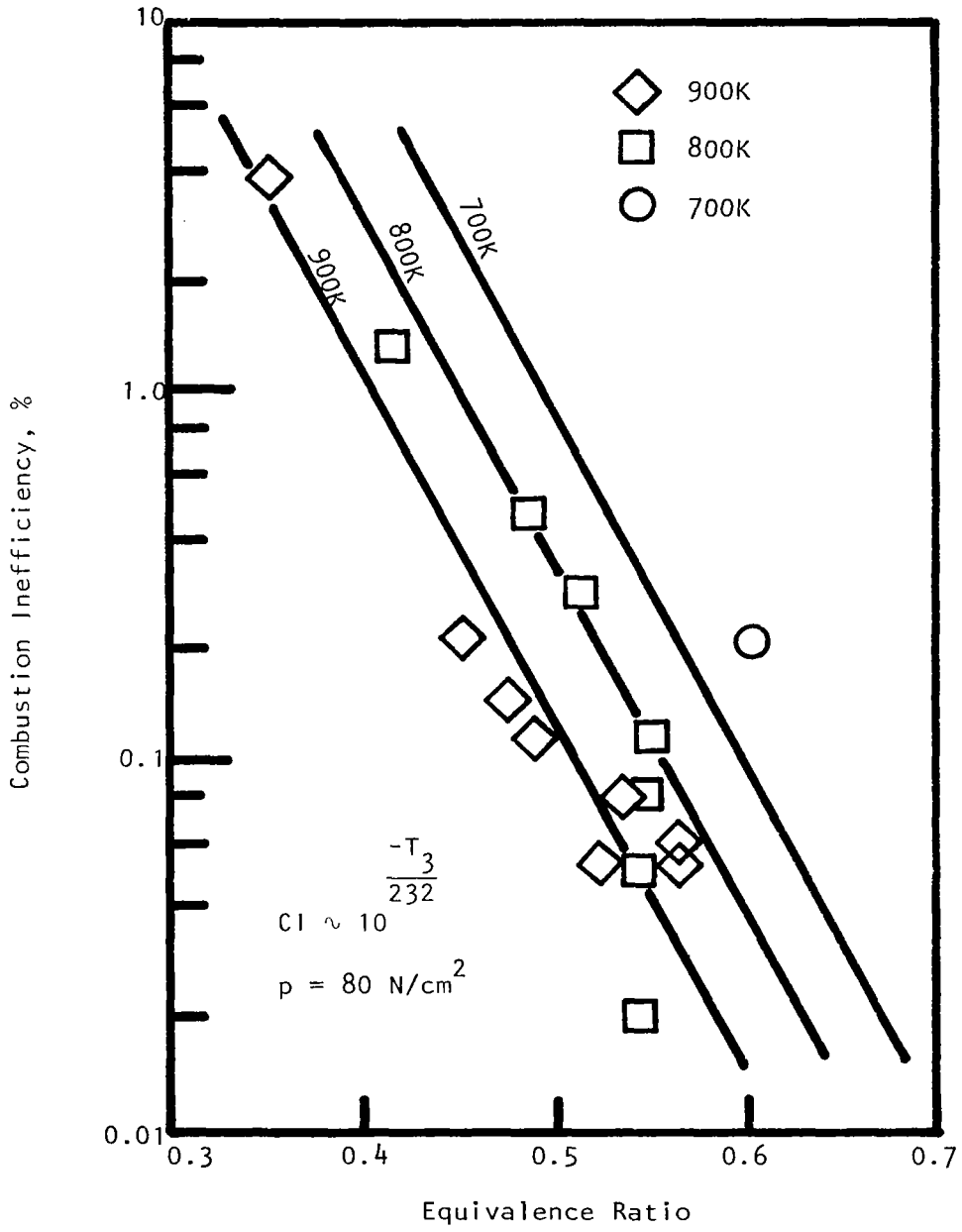


FIGURE 12b. COMBUSTION INEFFICIENCY AS A FUNCTION OF EQUIVALENCE RATIO AND COMBUSTOR INLET TEMPERATURE AT 80 N/cm$^2$

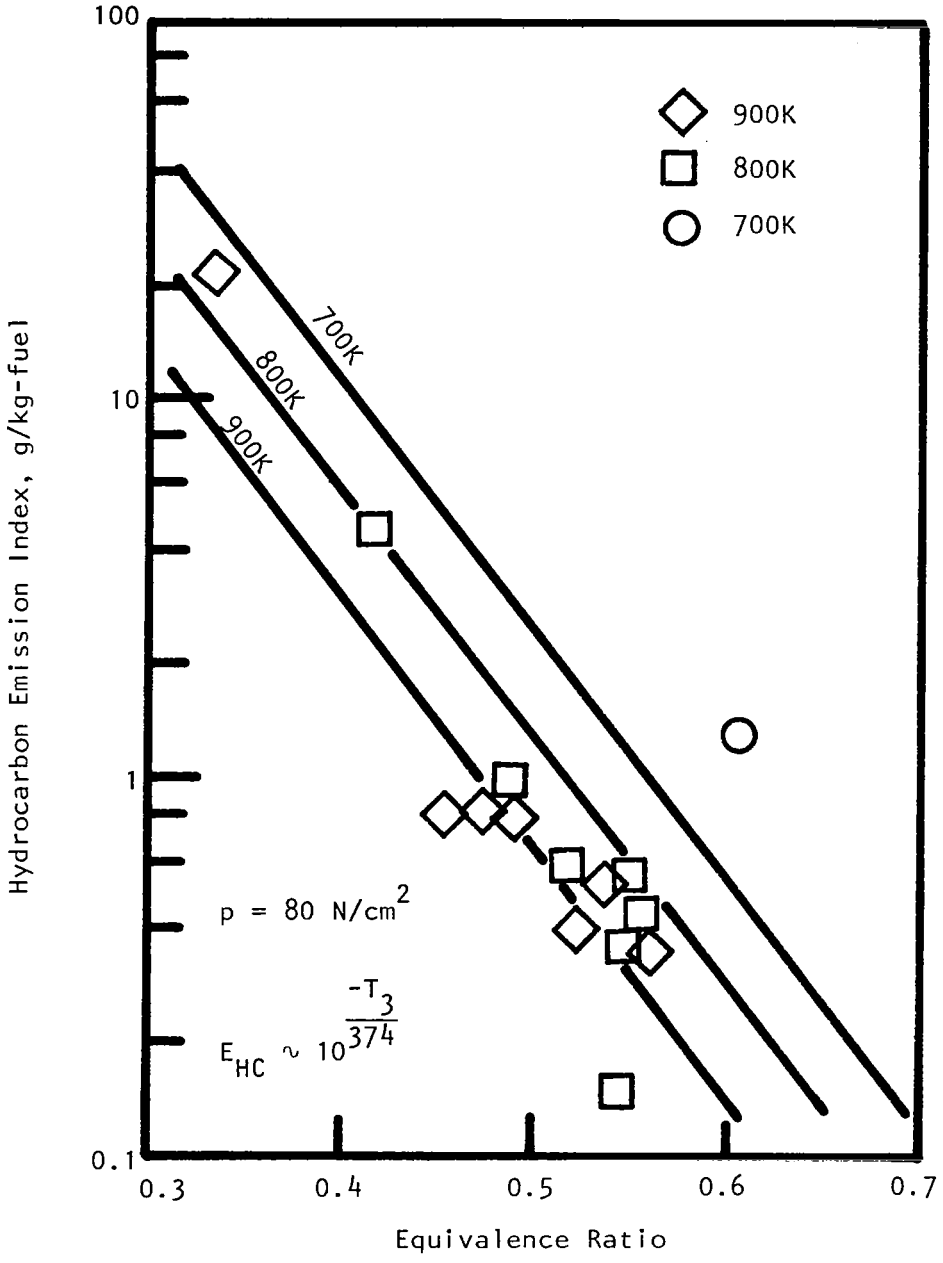


FIGURE 12c. HYDROCARBON EMISSION INDEX AS A FUNCTION OF EQUIVALENCE RATIO AND COMBUSTOR INLET TEMPERATURE AT 80 N/cm$^2$

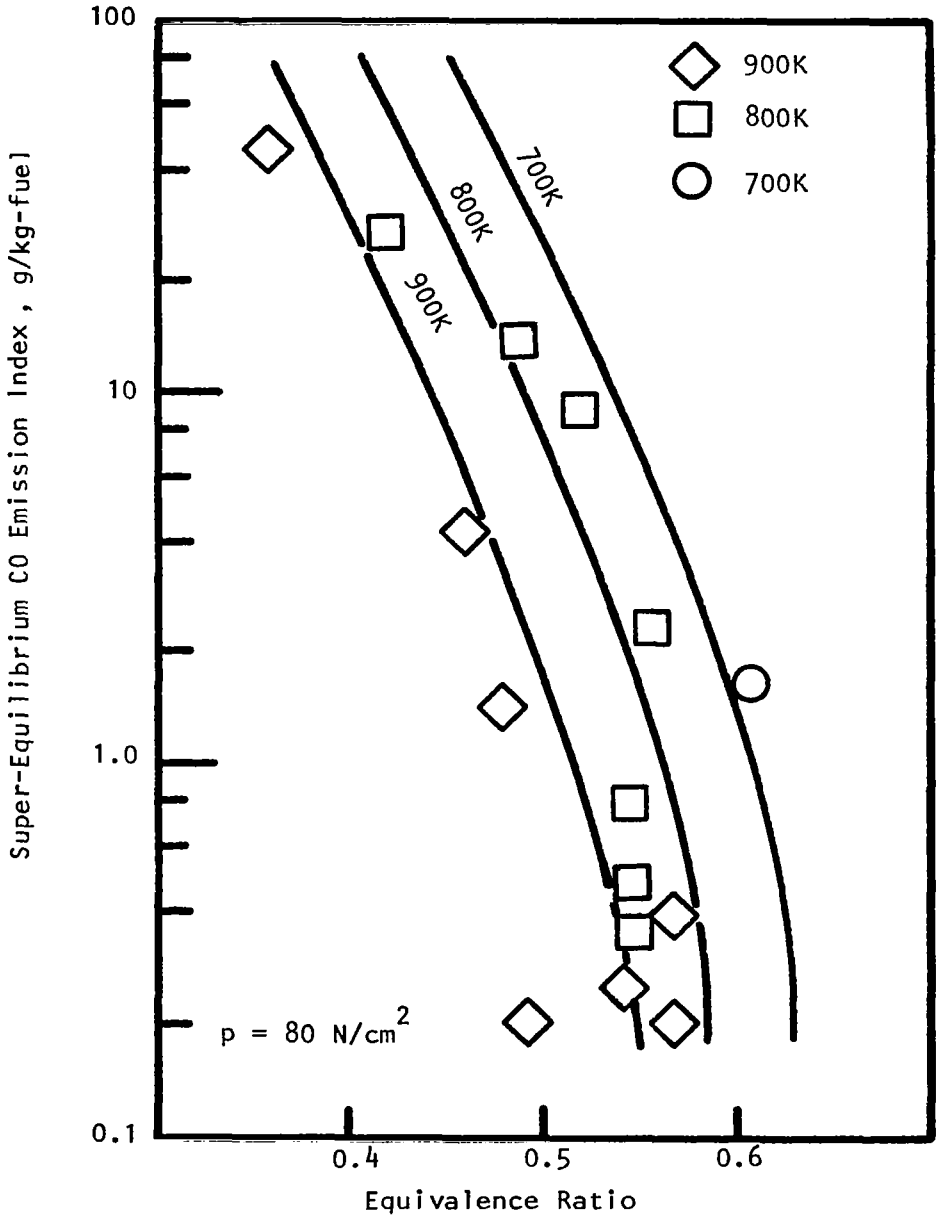


FIGURE 12d. SUPER-EQUILIBRIUM CARBON MONOXIDE EMISSION INDEX AS A FUNCTION OF EQUIVALENCE RATIO AND COMBUSTOR INLET TEMPERATURE AT 80 $N/cm^2$

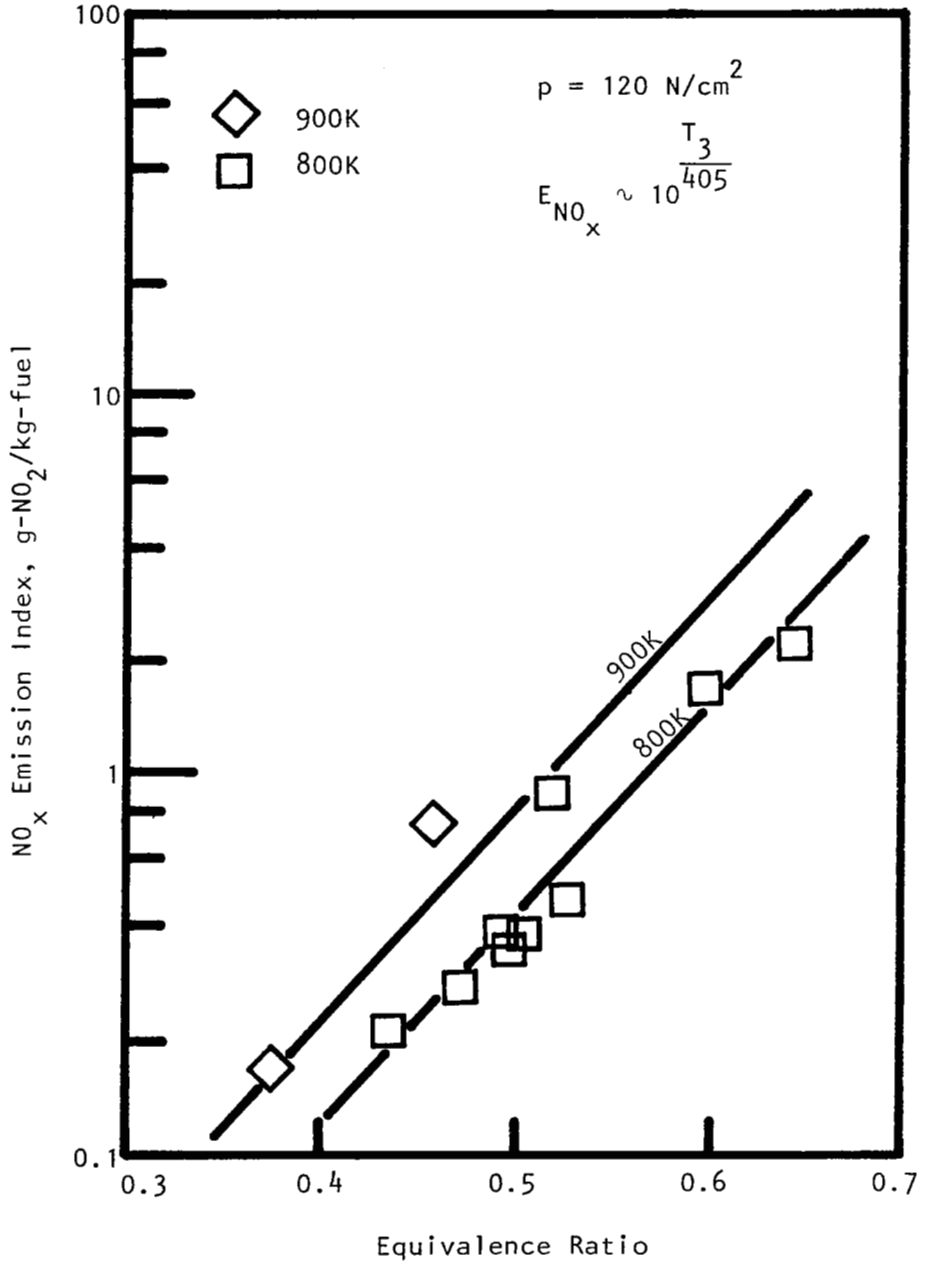


FIGURE 13a. $NO_x$ EMISSION INDEX AS A FUNCTION OF EQUIVALENCE RATIO AND COMBUSTOR INLET TEMPERATURE AT 120 N/cm$^2$

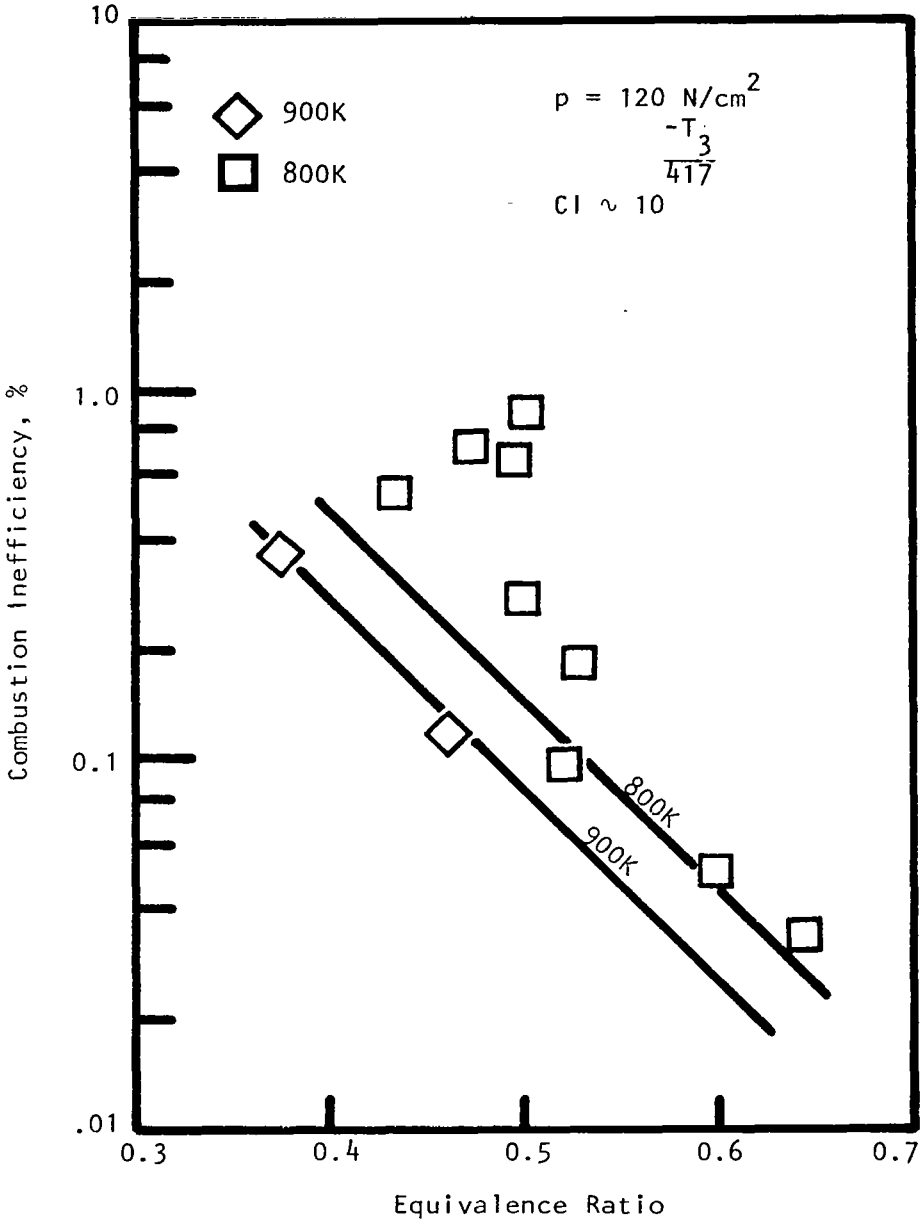


FIGURE 13b. COMBUSTION INEFFICIENCY AS A FUNCTION OF EQUIVALENCE RATIO AND COMBUSTOR INLET TEMPERATURE AT 120 N/cm$^2$

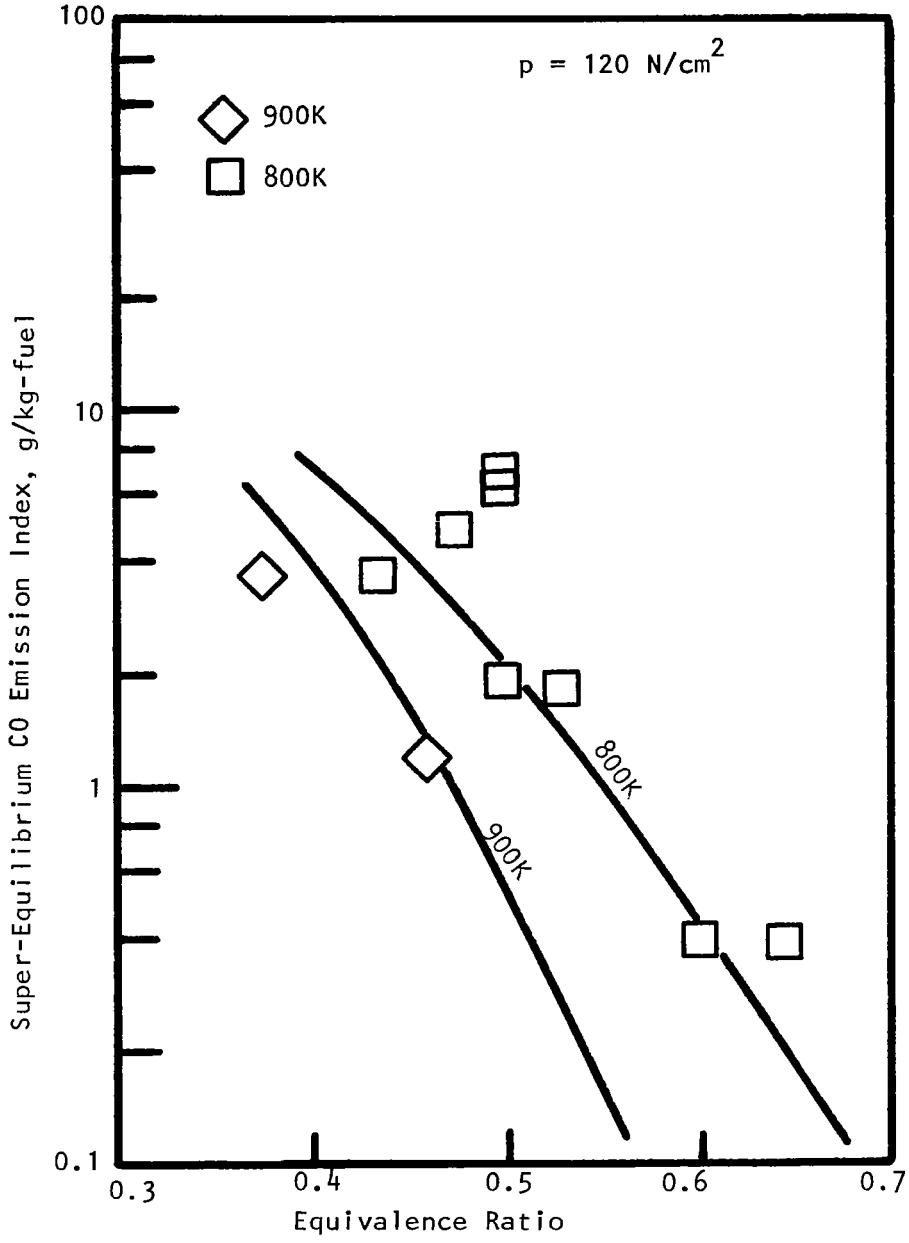


FIGURE 13c. HYDROCARBON EMISSION INDEX AS A FUNCTION OF EQUIVALENCE RATIO AND COMBUSTOR INLET TEMPERATURE AT 120 N/cm$^2$

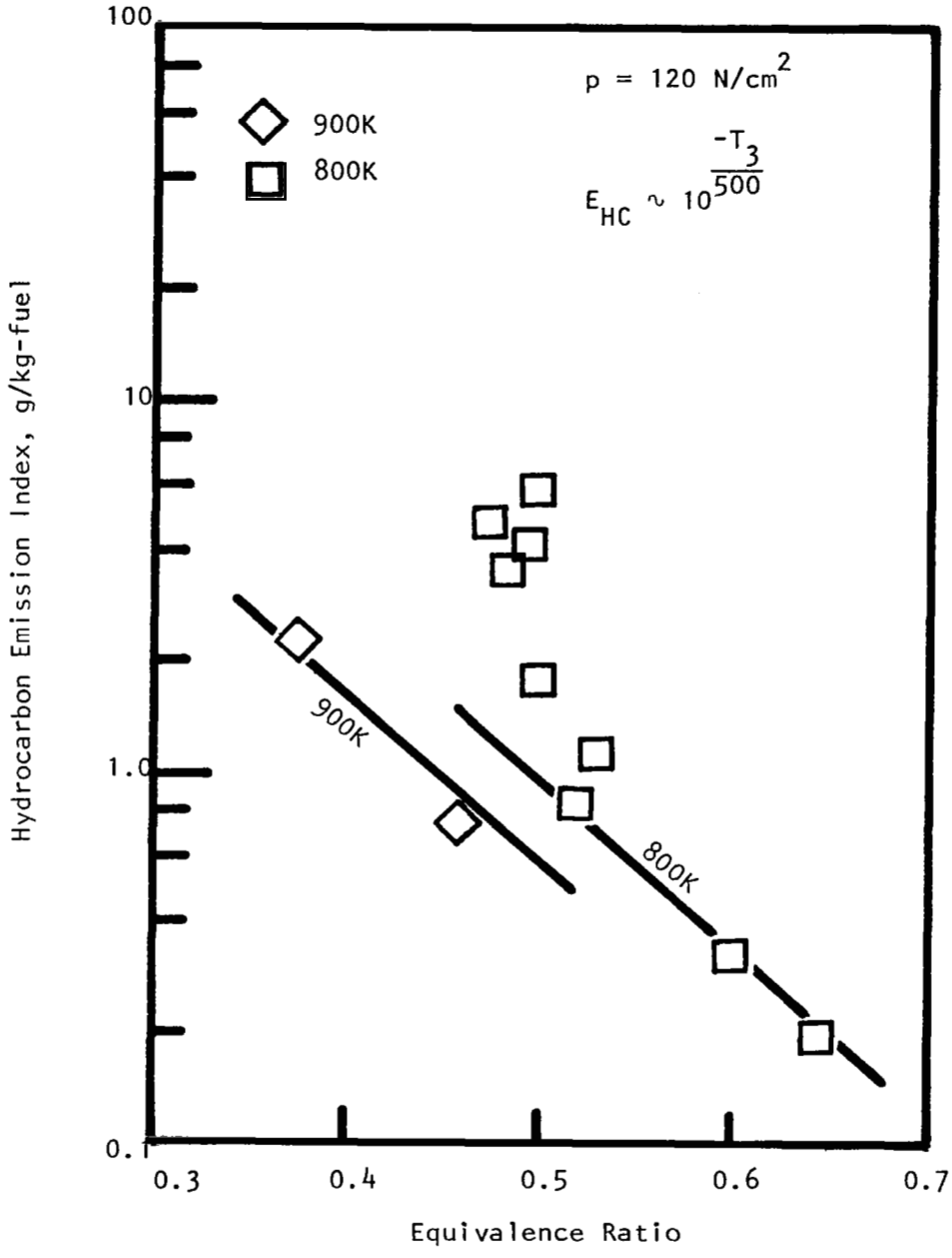


FIGURE 13d. SUPER-EQUILIBRIUM CARBON MONOXIDE EMISSION INDEX AS A FUNCTION OF EQUIVALENCE RATIO AND COMBUSTOR INLET TEMPERATURE AT 120 N/cm$^2$

The inlet temperature correction technique cannot be applied directly to the CO emission index, since this is a function of both adiabatic flame temperature and equivalence ratio. However, a super-equilibrium CO emission index can be defined based on the difference between measured CO concentration and equilibrium concentration. The advantage of the super-equilibrium index it that since it is derivable directly from the hydrocarbon emission index and the combustion inefficiency (see Appendix A) each of which are inlet temperature correctable, it too can be corrected for inlet temperature variation. The result for 40 $N/cm^2$ is presented in Figure (11d).

With the exception of the super-equilibrium CO emission index, the solid lines shown in each of the temperature-corrected data curves of Figures (11) through (13) are the equivalent of the solid lines drawn through the adiabatic flame temperature correlations presented in Figures (7) through (9). The solid lines drawn through the super-equilibrium CO data are a translation of the hydrocarbon emission index and combustion inefficiency curves using the definition of combustion inefficiency to derive super-equilibrium CO level. It is interesting to note that the data appear to fit the derived curves reasonably well, despite the considerable scatter evident in the adiabatic temperature correlations. The super-equilibrium CO emission index is not a pure exponential function of equivalence ratio as is the case for the other emission indices since the equilibrium CO level is a function of equivalence ratio as well as adiabatic flame temperature.

The principal significance of the two parameter combustor performance curves of Figures (11) through (13) is their usefulness in adjusting the lines drawn through the adiabatic temperature correlations, particularly for the low pressure cases where data scatter would permit considerable latitude in this regard. Interestingly, an error in the slope of the adiabatic temperature correlation results in a vertical stretching of the two parameter curves and a highly apparent mismatch between data points and solid lines. In the case of CO emission, the two parameter curves are the only way in which the data can be presented.

## CONCLUSIONS

By using an aerodynamically clean mixing duct to avoid local regions of separated flow which increase residence time above the 4 msec value characteristic of the bulk flow, it has been possible to operate a premixing combustor at pressures up to 120 $N/cm^2$ and combustor inlet temperatures up to 920K without encountering autoignition or flashback. Autoignition did occur in the mixing duct at a pressure of 240 $N/cm^2$ and a temperature of 833K.

The $NO_x$ and UHC emission indices and the combustion inefficiency correlate reasonably well with adiabatic flame temperature. Adiabatic flame temperatures between 1700K and 2200K produce $NO_x$ emission indices between 0.2 and 2.0 g-$NO_2$/kg-fuel. $NO_x$ levels measured at pressures of 40, 80 and 120 $N/cm^2$ vary somewhat from case to case. However, the degree of premixing produced by the normal injection design also varies and this effect could overshadow the pressure effects on reaction kinetics. Certainly, $NO_x$ levels are quite low at each of the three pressures tested.

At pressures of 40 and 80 $N/cm^2$, it was not possible to maintain stable combustion at adiabatic flame temperatures below 1700K. At a pressure of 120 $N/cm^2$, combustion inefficiency displayed behavior typical of incipient blow off at 1850K.

## REFERENCES


1. Roberts, R., Peduzzi, A. and Vitti, G., "Experimental Clean Combustor Program - Phase 1 Final Report," NASA CR-134736, October 1975.

2. Bahr, D. and Gleason, C., "Experimental Clean Combustor Program - Phase 1 Final Report," NASA CR-134737, June 1975.

3. Niedzwiecki, R. W. and Jones, R. E., "Parametric Test Results of a Swirl Can Combustor," NASA TMX-68247, June 1973.

4. Marek, C. J. and Papathakos, C., "Exhaust Emissions from a Premixing, Prevaporizing Flame Tube using Liquid Jet A Fuel," NASA TMX-3383, April 1976.

5. Roberts, P., Shekleton, J. and White, D., "Advanced Low $NO_x$ Combustors for Supersonic High-Altitude Aircraft Gas Turbines," ASME Paper 76-GT-12, Gas Turbine and Fluids Engineering Conference, March 1976.

6. Roffe, G. and Ferri, A., "Effect of Premixing Quality on Oxides of Nitrogen in Gas Tubine Combustors," NASA CR-2657, February 1976.

7. Roffe, G. and Ferri, A., "Prevaporization and Premixing to Obtain Low Oxides of Nitrogen in Gas Turbine Combustors," NASA CR-2495, March 1975.

8. "Procedure for the Continuous Sampling and Measurement of Gaseous Emissions from Aircraft Turbine Engines," Society of Automotive Engineers, ARP-1256, October 1971.

## APPENDIX A
## DATA REDUCTION PROCEDURES

The gas analysis instrumentation provide raw data in the form of volume fractions of the particular gases being sampled. This raw data is converted into the more convenient form of emission index and equivalence ratio following the procedures detailed below.

Each of the gas analysis instruments must be calibrated in order to convert the instrument reading to the volume fraction of the particular gas being analyzed. In the case of the Beckman Model 402 hydrocarbon analyzer and the Beckman Model 315B CO analyzer, this calibration is accomplished by passing prepared mixtures of calibration gas through the instruments and establishing calibration curves. The hydrocarbon analyzer was calibrated using gas standards containing 47 ppm, 91 ppm, 114 ppm and 269 ppm propane in nitrogen. The instrument output is proportional to the number of carbon atoms with hydrogen bonds. Thus, pure hydrogen or pure carbon will produce no response and a given concentration of propane ($C_3H_8$) will produce three times the response of an equal concentration of methane ($CH_4$). The instrument responds to all C-H bonds. As a result, it measures the sum of both unoxidized hydrocarbon and partially oxidized hydrocarbon molecules. The instrument calibration curve is shown in Figure (A1). The response is linear with hydrocarbon concentration, presented in units of ppmC, that is, the number of hydrogenated carbon atoms in parts per million.

Calibration of the Beckman Model 315B CO analyzer was accomplished using standard gases with 1530 ppm, 1043 ppm, 605 ppm, 305 ppm and 65 ppm CO in nitrogen. The calibration curve is shown in Figure (A2).

The gases used for calibration of the Beckman Model 864 $CO_2$ analyzer contained 10.2%, 5.0% and 2.0% $CO_2$ in nitrogen. The analyzer calibration curve is slightly nonlinear as shown in Figure (A3). The Beckman Model 951 $NO/NO_x$ analyzer was calibrated using standards containing 250 ppm, 216 ppm, 104 ppm, 82 ppm and 21 ppm $NO_x$ in nitrogen. The $NO_x$ analyzer produces a linear response as illustrated in Figure (A4).

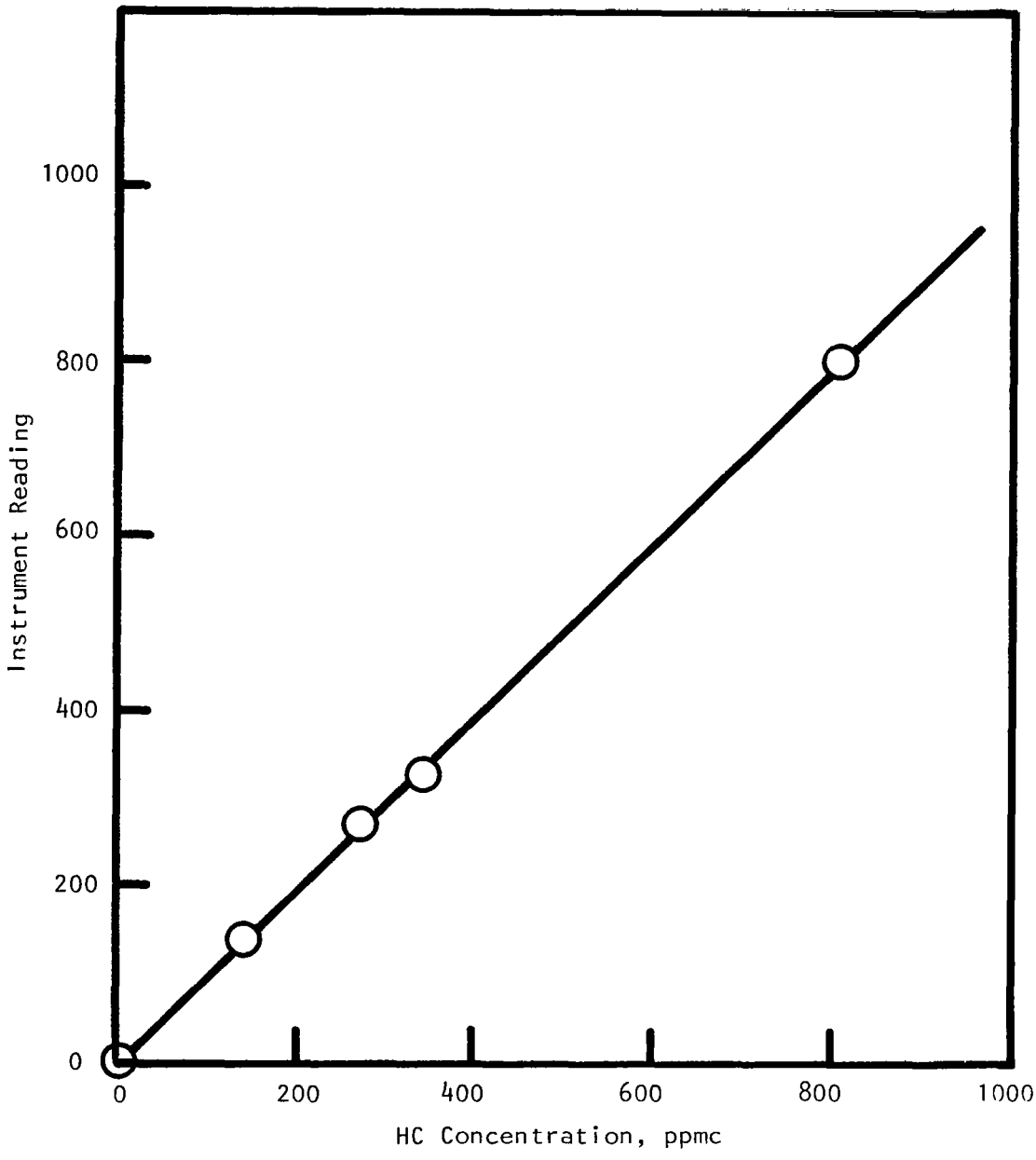


FIGURE A1. CALIBRATION OF BECKMAN MODEL 402 HYDROCARBON ANALYZER

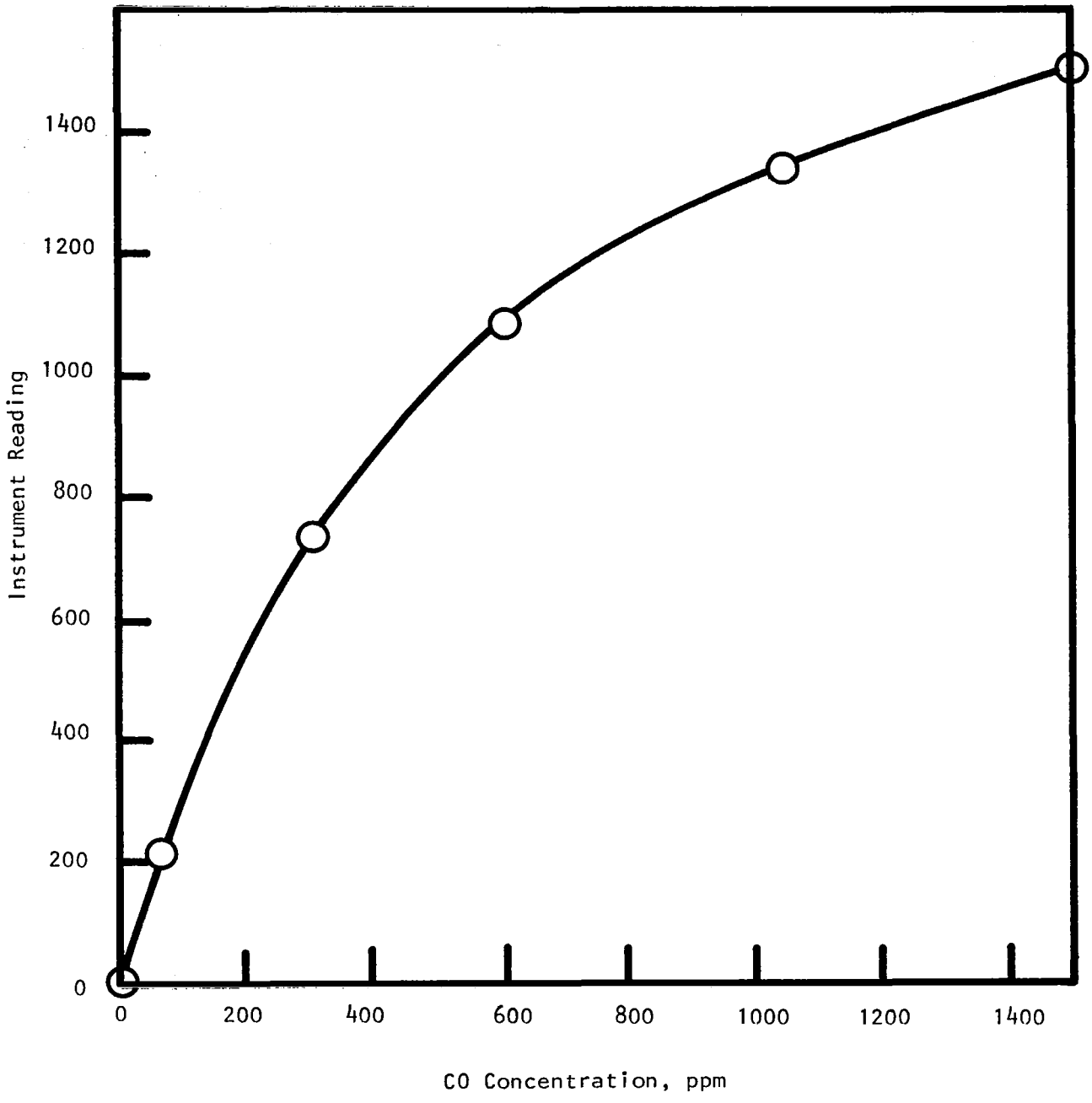


FIGURE A2. CALIBRATION OF BECKMAN 315B CO ANALYZER

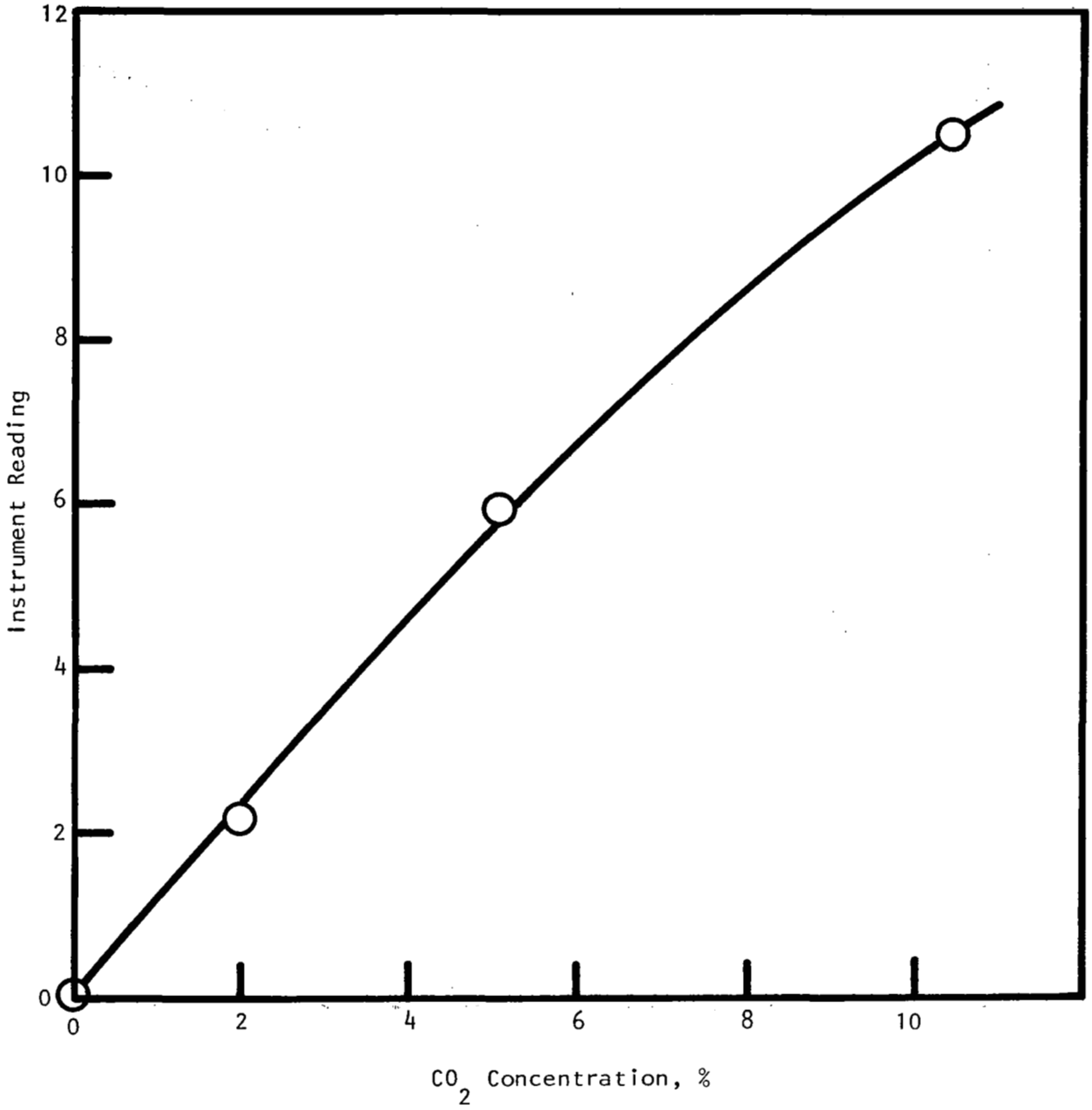


FIGURE A3. CALIBRATION CURVE FOR BECKMAN MODEL 864 $CO_2$ ANALYZER

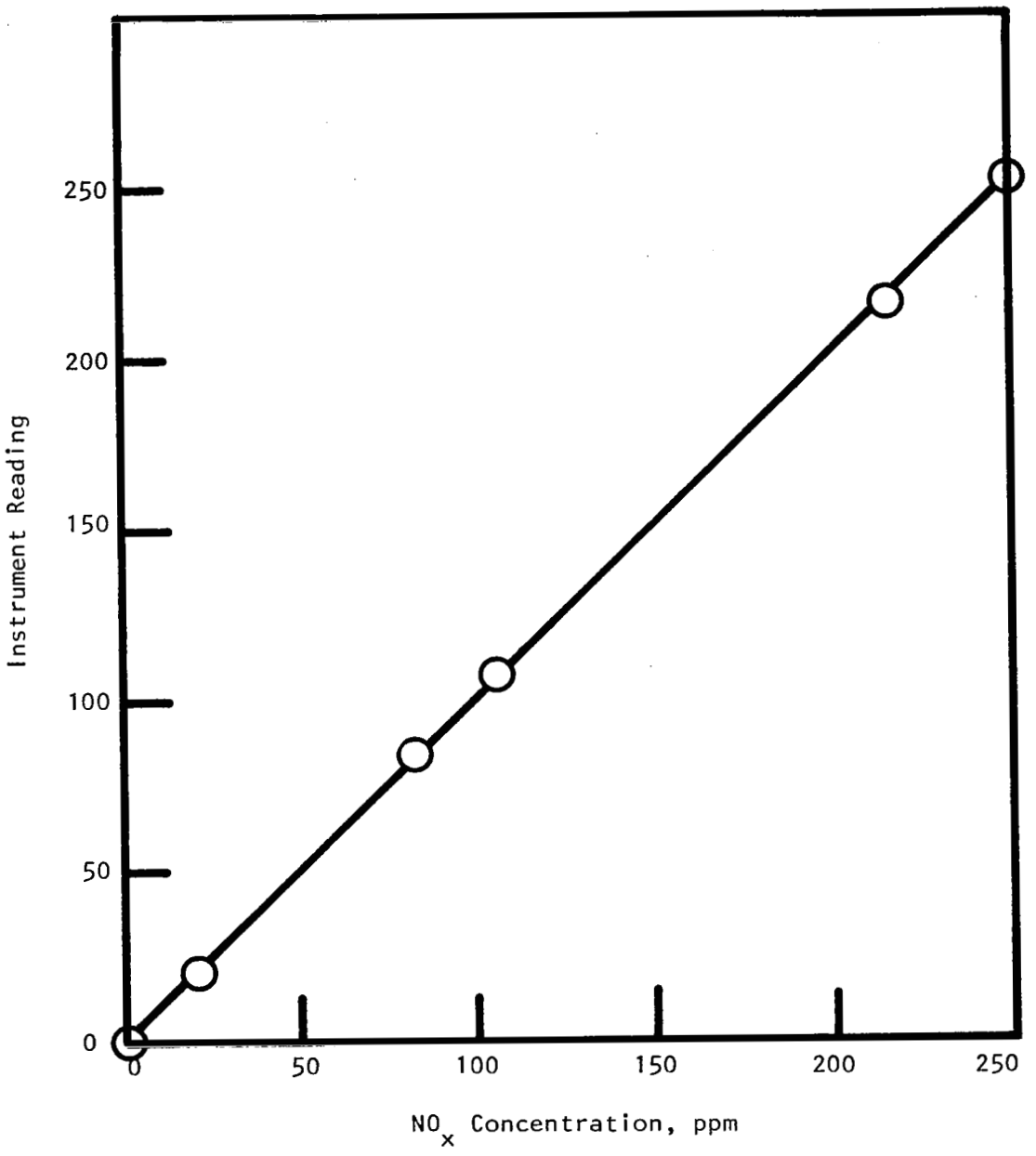


FIGURE A4. CALIBRATION OF BECKMAN MODEL 951 $NO/NO_x$ ANALYZER

The gas analysis instruments were calibrated once each week using the entire set of standard gases. Zero gas and span gas were passed through all instruments immediately prior to each test and the instrument output recorded on the same data roll which was used for the subsequent test run.

Conversion of the molar concentration (volume fractions) provided by the gas analysis instrumentation into the more convenient terms of emission index and equivalence ratio requires a prior knowledge of the ratio of carbon to hydrogen in the system. This is ascertained from a chemical analysis of the fuel used in the experiments. For the JP-5 fuel used here, the hydrogen to carbon ratio is 1.92 and the fuel/air ratio f/a is given by Reference (8) to be

$$f/a = \frac{CO \times 10^{-4} + CO_2 + HC \times 10^{-4}}{208 - 2.03 \times 10^{-4}\ CO - 0.998\ CO_2} \tag{A1}$$

where CO and HC are the molar concentrations of carbon monoxide and unburned hydrocarbon in units of parts per million (ppm) and ppmC respectively and $CO_2$ is the volume percent of carbon dioxide expressed as a percentage of total gas volume.

The equivalence ratio, $\phi$, is defined as the ratio of the actual fuel/air ratio to the stoichiometric fuel/air ratio. For JP-5,

$$\phi = 14.7\ (f/a) \tag{A2}$$

The combustion inefficiency, CI, is

$$CI = \frac{0.464\ CO + 1.11\ HC}{10^4\ CO_2 + CO + HC} \times 100$$

The numerator of the second term represents the potential heat release which could be obtained by further oxidation of CO to form $CO_2$ and hydrocarbons to form $H_2O$ and $CO_2$. However, a certain level of CO is required by chemical equilibrium considerations, this level being well represented by the following curve fit.

$$CO_{eq} = \frac{493}{\sqrt{p}}\ 10^{\left(\frac{\phi-0.6}{0.63} + \frac{T_4-1900}{230}\right)} \tag{A3}$$

where p is the pressure in $N/cm^2$ and $T_4$ is the adiabatic flame temperature in degrees Kelvin.

Since the production of the equilibrium CO level does not imply combustor inefficiency, the definition of percent combustion inefficiency CI is altered slightly so that a penalty accrues only from that portion of the total CO produced which exceeds the equilibrium value. Thus,

$$CI = \frac{0.464\ (CO-CO_{eq}) + 1.11\ HC}{10^{+4}\ CO_2 + CO + HC} \times 100 \qquad (A4)$$

The measured volume fractions expressed as ppm of CO, hydrocarbons and $NO_x$ are converted into emission indices (grams of component per kilogram of fuel) using the following expressions:

$$E_{CO} = \frac{CO\ (1 + f/a)}{1035\ f/a} \qquad (A5)$$

$$E_{HC} = \frac{HC\ (1 + f/a)}{2081\ f/a} \qquad (A6)$$

$$E_{NO_x} = \frac{NO_x (1 + f/a)}{630\ f/a} \qquad (A7)$$

In Equation (A7), the molecular weight of $NO_x$ is taken to be 46. This reflects the assumption that all NO produced eventually becomes $NO_2$. The emission index is thus based on the molecular weight of the $NO_2$ molecule. It is also convenient to define a super-equilibrium CO emission index, since this is representative of the first term in the numerator of the combustion inefficiency expression, Equation (A4). In this case

$$E_{CO_{supeq}} = \frac{(CO - CO_{eq})\ (1 + f/a)}{1035\ f/a} \qquad (A8)$$

## APPENDIX B

## DATA SUMMARY

| $P \times 10^{-1}$ ($N/cm^2$) | T (K) | $CO_2$ (%) | CO (ppm) | HC (ppmC) | $NO_x$ (ppm) | PHI | $ENO_x$ (g/kg) | ECO (g/kg) | EHC (g/kg) | CI (%) |
|---|---|---|---|---|---|---|---|---|---|---|
| 4.5 | 973 | 3.2 | 830 | 283 | 3 | 0.279 | 0.3 | 44.4 | 7.5 | 2.10 |
| 4.4 | 980 | 4.6 | 420 | 248 | 25 | 0.400 | 1.5 | 15.8 | 4.6 | 1.00 |
| 4.4 | 982 | 6.7 | 130 | 135 | 103 | 0.576 | 4.5 | 3.4 | 1.8 | 0.20 |
| 3.8 | 994 | 6.7 | 100 | 143 | 99 | 0.575 | 4.3 | 2.6 | 1.9 | 0.30 |
| 4.4 | 930 | 3.5 | 610 | 582 | 4 | 0.305 | 0.3 | 29.9 | 14.2 | 2.60 |
| 4.5 | 945 | 5.0 | 230 | 311 | 37 | 0.429 | 2.1 | 8.1 | 5.4 | 0.90 |
| 4.3 | 967 | 6.2 | 760 | 462 | 61 | 0.540 | 2.8 | 21.3 | 6.5 | 0.90 |
| 4.8 | 865 | 6.0 | 540 | 376 | 15 | 0.520 | 0.7 | 15.7 | 5.4 | 1.00 |
| 4.8 | 849 | 6.7 | 530 | 347 | 22 | 0.581 | 0.9 | 13.9 | 4.5 | 0.60 |
| 4.6 | 808 | 6.3 | 900 | 490 | 14 | 0.550 | 0.6 | 24.8 | 6.7 | 1.40 |
| 4.5 | 814 | 6.6 | 830 | 530 | 35 | 0.576 | 1.5 | 21.9 | 6.9 | 1.20 |
| 4.4 | 824 | 5.4 | 650 | 470 | 13 | 0.469 | 0.7 | 20.9 | 7.5 | 1.50 |
| 4.7 | 822 | 6.0 | 775 | 500 | 26 | 0.523 | 1.2 | 22.5 | 7.2 | 1.40 |
| 4.5 | 789 | 4.7 | 1700 | 1210 | 2 | 0.423 | 0.1 | 60.4 | 21.4 | 4.30 |
| 4.6 | 781 | 4.6 | 420 | 597 | 2 | 0.394 | 0.2 | 16.0 | 11.3 | 1.80 |
| 4.6 | 779 | 5.5 | 830 | 700 | 11 | 0.481 | 0.6 | 26.1 | 10.9 | 2.00 |
| 4.5 | 767 | 6.6 | 1380 | 974 | 23 | 0.581 | 1.0 | 36.1 | 12.7 | 2.40 |
| 4.5 | 737 | 6.8 | 1510 | 1070 | 26 | 0.605 | 1.1 | 38.0 | 13.4 | 2.40 |
| 4.5 | 749 | 6.9 | 1530 | 1210 | 44 | 0.615 | 1.8 | 37.9 | 14.9 | 2.50 |
| 4.4 | 747 | 6.6 | 1800 | 1320 | 33 | 0.592 | 1.4 | 46.2 | 16.9 | 3.10 |
| 4.6 | 806 | 6.7 | 1030 | 520 | 13 | 0.591 | 0.5 | 26.5 | 6.7 | 1.20 |
| 4.6 | 803 | 7.2 | 1030 | 501 | 23 | 0.636 | 0.9 | 24.7 | 6.0 | 0.80 |
| 4.5 | 789 | 6.0 | 1250 | 694 | 5 | 0.529 | 0.2 | 35.8 | 9.9 | 2.10 |
| 4.4 | 782 | 5.8 | 1350 | 781 | 3 | 0.516 | 0.1 | 39.6 | 11.4 | 2.40 |
| 4.3 | 769 | 4.5 | 1900 | 1240 | 3 | 0.408 | 0.2 | 70.0 | 22.7 | 4.70 |
| 4.5 | 735 | 6.1 | 1800 | 1210 | 4 | 0.543 | 0.2 | 50.3 | 16.8 | 3.40 |
| 4.9 | 721 | 6.1 | 1800 | 1240 | 6 | 0.547 | 0.3 | 49.9 | 17.1 | 3.40 |
| 8.0 | 908 | 5.7 | 60 | 50 | 5 | 0.491 | 0.27 | 1.8 | 0.8 | 0.10 |
| 8.0 | 908 | 6.3 | 40 | 38 | 15 | 0.539 | 0.71 | 1.1 | 0.5 | 0.07 |
| 8.0 | 908 | 6.6 | 35 | 29 | 34 | 0.565 | 1.50 | 0.9 | 0.4 | 0.06 |

| $Px10^{-1}$ ($N/cm^2$) | T (K) | $CO_2$ (%) | CO (ppm) | HC (ppmC) | $NO_x$ (ppm) | PHI | $ENO_x$ (g/kg) | ECO (g/kg) | EHC (g/kg) | CI (%) |
|---|---|---|---|---|---|---|---|---|---|---|
| 8.0 | 903 | 6.6 | 40 | 27 | 20 | 0.565 | 0.87 | 1.1 | 0.4 | 0.05 |
| 8.0 | 882 | 5.4 | 190 | 55 | 3 | 0.457 | 0.17 | 6.3 | 0.9 | 0.25 |
| 8.0 | 838 | 4.9 | 450 | 218 | 2 | 0.420 | 0.13 | 16.1 | 3.9 | 0.90 |
| 8.0 | 862 | 3.8 | 2000 | 1320 | 3 | 0.353 | 0.19 | 84.8 | 27.8 | 5.72 |
| 8.7 | 840 | 5.7 | 320 | 51 | 2 | 0.489 | 0.08 | 9.9 | 0.8 | 0.32 |
| 8.6 | 830 | 6.1 | 300 | 33 | 2 | 0.519 | 0.09 | 8.8 | 0.5 | 0.23 |
| 8.6 | 810 | 6.4 | 55 | 10 | 4 | 0.547 | 0.20 | 1.5 | 0.1 | 0.02 |
| 8.6 | 782 | 6.4 | 230 | 37 | 5 | 0.553 | 0.25 | 6.3 | 0.5 | 0.14 |
| 8.6 | 760 | 6.1 | 1350 | 357 | 4 | 0.536 | 0.18 | 38.2 | 5.0 | 1.58 |
| 8.6 | 735 | 6.3 | 1020 | 353 | 2 | 0.550 | 0.10 | 28.1 | 4.8 | 1.29 |
| 8.2 | 886 | 5.6 | 110 | 59 | 4 | 0.478 | 0.22 | 3.5 | 0.9 | 0.16 |
| 8.1 | 855 | 6.1 | 80 | 38 | 8 | 0.526 | 0.37 | 2.3 | 0.5 | 0.07 |
| 8.3 | 822 | 6.4 | 120 | 34 | 9 | 0.548 | 0.40 | 3.3 | 0.5 | 0.06 |
| 8.3 | 794 | 6.4 | 60 | 27 | 9 | 0.547 | 0.40 | 1.7 | 0.4 | 0.05 |
| 8.2 | 749 | 7.1 | 245 | 82 | 17 | 0.607 | 0.71 | 6.1 | 1.0 | 0.13 |
| 12.0 | 921 | 4.5 | 100 | 93 | 3 | 0.378 | 0.18 | 4.0 | 1.8 | 0.33 |
| 12.0 | 870 | 5.4 | 52 | 58 | 12 | 0.460 | 0.62 | 1.7 | 0.9 | 0.14 |
| 12.0 | 837 | 6.1 | 45 | 40 | 23 | 0.521 | 1.10 | 1.3 | 0.6 | 0.08 |
| 12.0 | 802 | 7.0 | 40 | 26 | 41 | 0.600 | 1.70 | 1.0 | 0.3 | 0.05 |
| 12.0 | 769 | 7.5 | 39 | 22 | 47 | 0.645 | 1.83 | 0.9 | 0.3 | 0.04 |
| 12.0 | 767 | 5.8 | 95 | 529 | 6 | 0.499 | 0.29 | 2.9 | 8.0 | 1.06 |
| 12.0 | 752 | 5.8 | 70 | 420 | 6 | 0.494 | 0.28 | 2.1 | 6.4 | 0.85 |
| 12.0 | 796 | 5.1 | 95 | 217 | 4 | 0.436 | 0.21 | 3.3 | 3.7 | 0.55 |
| 12.0 | 777 | 5.9 | 60 | 149 | 6 | 0.500 | 0.32 | 1.8 | 2.2 | 0.31 |
| 12.0 | 755 | 6.2 | 75 | 121 | 7 | 0.531 | 0.35 | 2.1 | 1.7 | 0.24 |
| 12.0 | 780 | 5.6 | 110 | 365 | 5 | 0.476 | 0.25 | 3.5 | 5.8 | 0.80 |
| 12.0 | 728 | 5.7 | 140 | 365 | 4 | 0.491 | 0.20 | 4.3 | 5.6 | 0.80 |